Monthly Notices
of the
ROYAL ASTRONOMICAL SOCIETY

MNRAS **492,** 2418–2436 (2020)
Advance Access publication 2019 November 14

doi:10.1093/mnras/stz2909

The $I\kappa\epsilon\alpha$ model of feedback-regulated galaxy formation

Mahavir Sharma [1,2]★ and Tom Theuns [3]

[1] *International Centre for Radio Astronomy Research (ICRAR), Curtin University, Bentley, WA 6102, Australia*
[2] *ARC Centre of Excellence for All Sky Astrophysics in 3 Dimensions (ASTRO 3D), Australia*
[3] *Institute for Computational Cosmology, Department of Physics, Durham University, Durham DH1 3LE, UK*

Accepted 2019 October 7. Received 2019 October 7; in original form 2019 June 24

ABSTRACT

We present the $I\kappa\epsilon\alpha$ model of galaxy formation, in which a galaxy's star formation rate is set by the balance between energy injected by feedback from massive stars and energy lost by the deepening of the potential of its host dark matter halo due to cosmological accretion. Such a balance is secularly stable provided that the star formation rate increases with the pressure in the star-forming gas. The $I\kappa\epsilon\alpha$ model has four parameters that together control the feedback from star formation and the cosmological accretion rate on to a halo. $I\kappa\epsilon\alpha$ reproduces accurately the star formation rate as a function of halo mass and redshift in the EAGLE hydrodynamical simulation, even when all the four parameters are held constant. It predicts the emergence of a star-forming main sequence along which the specific star formation rate depends weakly on stellar mass with an amplitude that increases rapidly with redshift. We briefly discuss the emerging mass–metallicity relation, the evolution of the galaxy stellar mass function, and an extension of the model that includes feedback from active galactic nuclei. These self-regulation results are independent of the star formation law and the galaxy's gas content. Instead, star-forming galaxies are shaped by the balance between stellar feedback and cosmological accretion, with accurately accounting for energy losses associated with feedback as a crucial ingredient.

Key words: galaxies: evolution – galaxies: formation – galaxies: general – quasars: supermassive black holes.

1 INTRODUCTION

The cold dark matter cosmogony links the small fluctuations detected in the cosmic microwave background (CMB) at redshift $z \sim 1000$ to the observed large-scale clustering of galaxies at all observable redshifts. The fluctuations in the CMB temperature correspond to density perturbations that grow in amplitude due to gravity, resulting in the formation of dark matter haloes that host galaxies (see e.g. Springel et al. 2005, and reference therein for more background).

Whereas computer simulations can reliably predict virtually all properties of dark haloes, the same cannot be said for the properties of the galaxies that inhabit these haloes. Even though our basic understanding of the underlying physics is probably correct – galaxies form as gas accretes on to a halo, cools, becomes self-gravitating, and forms stars (White & Rees 1978; White & Frenk 1991) – numerous uncertainties remain. What sets the star formation rate of a galaxy in a given halo at a given redshift? How does the energetic feedback from stars and accreting black holes regulate star formation? What is the role of galaxy interactions such as mergers? Are there any other crucial processes, for example feedback from cosmic rays or reionization, and what is the role of magnetic fields?

Models that are designed to reproduce a mock universe that looks and evolves like the one we observe may not care about the details of the relevant physical processes. Examples include halo occupation distribution models (HOD; e.g. Peacock & Smith 2000) or subhalo abundance matching [SHAM; e.g. Vale & Ostriker (2004), see e.g. Wechsler & Tinker (2018) for recent reviews].

Semi-analytical models recognize that the physics of galaxy formation is complex, and use parametrizations to model poorly understood physical processes. Cosmological hydrodynamical simulations try to capture some of these physical processes as accurately as possible (cosmological accretion and cooling of gas on to haloes for example), but also rely on more parametrized descriptions of physical processes to capture physics below the resolution scale (see Somerville & Davé 2015 and Naab & Ostriker 2017, for recent reviews).

Several of the semi-analytical models and recent hydrodynamical simulations yield a mock universe that looks impressively similar to the one observed. Even though these models typically all include the same ingredients, the details of how the processes are implemented may be quite different. It is therefore somewhat surprising that the resulting galaxy population is nevertheless very similar. At the very

★ E-mail: mahavir.sharma@curtin.edu.au

least, this suggests some level of degeneracy in the modelling and that such calculations cannot be used to infer how the unresolved processes operate in detail. But it also suggests that many properties of galaxies do not actually depend on the details of many of these processes (see Hopkins et al. 2014, for a similar point of view).

Arguably, one of the more striking features of the galaxy population as a whole is the emergence of a 'star-forming main sequence' (or 'blue cloud'), Noeske et al. (2007), on which galaxies form stars at a specific rate, $\dot{M}_\star/M_\star$, that depends weakly on stellar mass ($M_\star$), but increases rapidly with redshift. The scatter around the mean trend is small, of the order of 0.3 dex (see Schreiber et al. 2015, and references therein for more recent observational analysis and discussion).

The appearance of such a main sequence suggests that the rate at which a galaxy forms stars in a halo of given mass is somehow self-regulating. Several papers argued just that (e.g. Bouché et al. 2010; Davé, Finlator & Oppenheimer 2012; Dayal, Ferrara & Dunlop 2013; Lilly et al. 2013; Dekel & Mandelker 2014). The aim of these models is not to be able to predict the properties of galaxies in great detail, but rather understand the origin of self-regulation. This paper follows this philosophy, adopting simplifications to more clearly expose the feedback loop that operates on the star-forming sequence.

This paper is organized as follows. Section 2 exposes the basic physics behind self-regulation in our model and tests the central assumptions by comparing to galaxies from the EAGLE (Evolution and Assembly of Galaxies and their Environments) cosmological hydrodynamical simulation (Schaye et al. 2015). Section 3 explores consequences in terms of galaxy scaling relations [such as the galaxy stellar mass function (GSMF) and the mass–metallicity relation], compares these to simulations and data, and discusses successes and failures of the model. Section 4 puts our results into context by comparing to previous work, and discusses what we think are its main limitations. Section 5 summarizes our findings and is followed by an appendix that contains a short overview of the EAGLE simulations, including a description of the reference model, 'Ref-L100N1504', in which the subgrid parameters are calibrated to reproduce redshift $z = 0$ observations of the GSMF, the relation between galaxy size and mass, and the relation between black hole mass and stellar mass, as described by Crain et al. (2015). The appendix also describes the EAGLE model 'FbConstNoAGN', in which the feedback parameters are kept constant and which does not include feedback from an active galactic nucleus (AGN), as well as another EAGLE variation, 'FbConst', in which the feedback parameters are kept constant and which does include AGN feedback.

2 SELF-REGULATION OF STAR FORMATION IN GALAXIES

The appearance of a star-forming sequence of galaxies is suggestive of the action of a feedback cycle. Such a feedback cycle is also important in understanding the main sequence of *stars* in a Hertzsprung–Russel diagram. Indeed, nuclear energy generation in main-sequence stars is secularly stable – a prerequisite for their longevity. We begin this section by briefly describing the well-known reason behind this stability (see e.g. any text book on stellar structure, for example Prialnik 2009). We next investigate whether we can apply similar reasoning to star-forming galaxies.

2.1 The secular evolution of main-sequence stars

The total energy E of a main-sequence star of mass M is the sum of its gravitational energy, $\Omega < 0$, and its internal energy, $U = Mu$, where u is its mean specific energy per unit mass. Stars are approximately in virial equilibrium, $E = \Omega/2 = -Mu$, and as a consequence $\mathrm{d}E/\mathrm{d}u < 0$. Therefore, if a star loses energy, for example, through radiation so that $\dot{E} < 0$, it will *heat up*, $\dot{u} > 0$. The effective negative specific heat capacity of a star is well known but nevertheless an intriguing feature of gravitationally bound systems, see e.g. Lynden-Bell & Lynden-Bell (1977), and is crucial for its longevity.

Indeed, consider a star losing energy through radiation (rate L), while gaining internal energy through nuclear fusion (rate $\dot{E}_\mathrm{nucl}$),

$$\dot{E} = \dot{E}_\mathrm{nucl} - L. \tag{1}$$

In equilibrium, $\dot{E} = 0$, however consider what happens for (small) deviations from equilibrium. Assuming $\dot{E}_\mathrm{nucl} < L$, say, $|E|$ increases since $E < 0$, meaning $|u|$ increases and hence the temperature T rises. The rate of energy generation through fusion is a rapidly increasing function of T, hence increasing T increases $\dot{E}_\mathrm{nucl}$, so that $\dot{E}_\mathrm{nucl} < L$ results in an increase in $\dot{E}_\mathrm{nucl}$ towards equilibrium. Similarly, if $\dot{E}_\mathrm{nucl} > L$, the decrease in T results in a decrease in the nuclear burning, until $\dot{E}_\mathrm{nucl} = L$. Clearly, the negative specific heat capacity of a star is not just an amusing feature of self-gravitating systems, but is key in understanding stability on the main sequence. As the star's mean molecular weight changes due to fusion, L and hence $\dot{E}_\mathrm{nucl}$ evolve secularly on a time-scale that vastly exceeds E/L.

2.2 The evolution of a galactic halo

As a galactic halo[1] grows in mass due to cosmological accretion, its energy changes in time as well. At first sight, there is little in common between the evolution of a galactic halo and that of a main-sequence star. Indeed, the total energy of a star changes only secularly, $|\dot{E}| \ll L$, as self-regulation leads to a near-balance between the energy generated by nuclear fusion and lost by radiation, but a galactic halo seems to have no equivalent channel for regulation. Does that mean that it is not secularly stable? The answer is partially yes: We show in the following that the dark matter halo is not secularly stable, in the sense that $\dot{E}_\mathrm{h} \neq 0$. However, the same may not be true for the galaxy itself, because supernovae inject energy into the interstellar medium (ISM). Below, we investigate whether that energy injection rate balances the loss of energy due to cosmological accretion, and if such a situation is a stable equilibrium – in analogy with the evolution of main-sequence stars described above. Before we do so, we summarize some well-known relations for the evolution of dark matter haloes.

2.3 The growth of a dark matter halo

We begin by investigating the cosmological growth in mass and the associated change in energy of a dark matter halo. The concentration and mass of a dark matter halo may be affected by baryonic processes. Indeed, in the simulations presented by Duffy et al. (2010), strong cooling and inefficient feedback increase the central dark matter density of galaxy and group haloes significantly, whereas strong feedback, for example from an AGN, *decreases* that density. Baryonic mass-loss, associated with strong feedback, may lead to a decrease in the rate at which a dark matter halo increases its mass. These effects are relatively modest at the scale

[1] We will use the term 'galactic halo' to refer to a central galaxy (as opposed to a satellite galaxy) with gas and stars, together with its host dark matter halo.

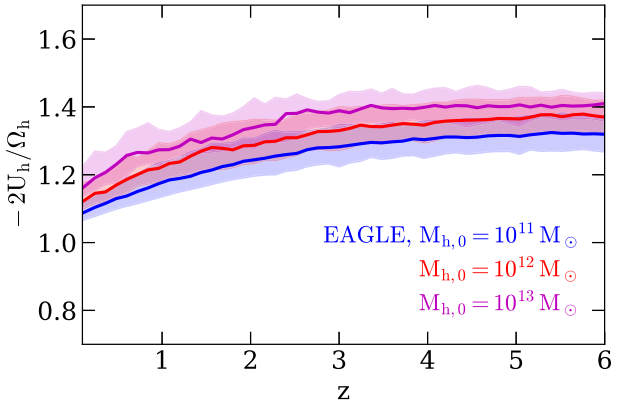

Figure 1. The redshift evolution of the virial ratio, $-2U_h/\Omega_h$, of dark matter haloes from the EAGLE L100N1504 dark matter-only simulation tracked along their merger tree. Here, U_h is the sum of the kinetic energy of all particles in the centre of mass rest frame, and Ω_h is the gravitational energy. Different colours refer to haloes in narrow bins of their $z = 0$ halo mass $M_{h,0}$: *blue*, *red*, and *purple* correspond to $M_{h,0} = [0.98–1.02] \times 10^{11}$, $[0.9–1.1] \times 10^{13}$, and $[0.8–1.2] \times 10^{13}$ $M_\odot$, respectively; the solid curves are the median value of the virial ratio, and the shaded region encompasses the 25–75th percentiles. Haloes evolve approximately in virial equilibrium.

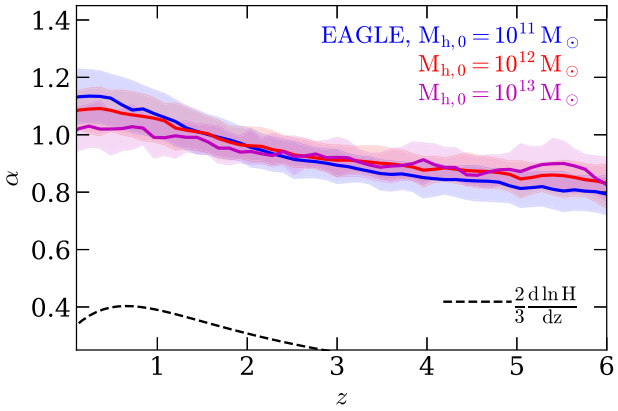

Figure 2. As Fig. 1 but for the concentration parameter α from equation (2). As a halo grows, α remains approximately constant. The *dashed curve* quantifies the (negligible) effect of the last term on the right-hand side in equation (4).

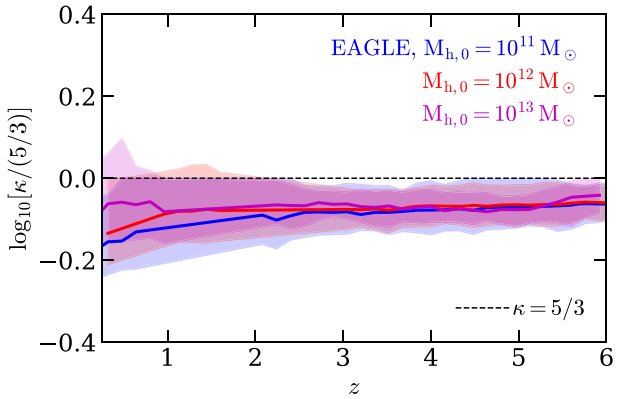

Figure 3. As Fig. 1 but for $\kappa = \mathrm{d}(\ln|E_h|)/\mathrm{d}(\ln M_h)$, where E_h and M_h are the total energy and mass of a halo from equation (2).

of galaxies in the EAGLE simulations, as shown by Schaller et al. (2015), and we will neglect them in this paper.

The total energy, $E_h < 0$, of a dark matter halo with mass M_h is the sum of its potential energy, $\Omega_h < 0$, and its internal energy, U_h (the total kinetic energy of all dark matter particles in the centre of mass rest frame, subscript h for halo). Dark matter haloes satisfy the virial theorem approximately, $E_h \approx \Omega_h/2 \approx -U_h$ (e.g. Neto et al. 2007), as we show in Fig. 1. There is clearly some evolution of the ratio U_h/Ω_h as the halo grows, but we will neglect this in what follows.

Assuming that the dark matter halo is in virial equilibrium, mass, radius, and internal energy are related by

$$\begin{aligned} E_h &= \Omega_h + U_h = \frac{\Omega_h}{2} = -U_h \\ \Omega_h &= -\alpha \frac{G\,M_h^2}{R_h} \\ U_h &= \frac{1}{2} M_h\, {v_h}^2 \\ R_h &= \left(\frac{G M_h}{100\,H^2}\right)^{1/3}. \end{aligned} \tag{2}$$

We used the standard way of assigning a 'radius', R_h, to a halo, by requiring that the mean density within R_h is 200 times the critical density, $\rho_c = 3H^2/(8\pi G)$, where $H(z)$ is the Hubble constant at redshift z. The value of the dimensionless parameter α depends on the halo's density profile: $\alpha = 3/5$ for constant density, $\alpha = R_h/(6a)$ for the spherical profile with scale radius a described by Hernquist (1990), and α is uniquely related to the concentration parameter, c, of a halo with a NFW (Navarro, Frenk & White 1997) profile. Equations (2) also define a characteristic 'virial velocity' of the halo, v_h, also given by

$${v_h}^2 = \alpha\,(G M_h)^{2/3} (10H)^{2/3}. \tag{3}$$

If the accreting halo remains in virial equilibrium, then

$$\frac{\mathrm{d}\ln|E_h|}{\mathrm{d}z} = \frac{5}{3}\frac{\mathrm{d}\ln M_h}{\mathrm{d}z} + \frac{\mathrm{d}\ln\alpha}{\mathrm{d}z} + \frac{2}{3}\frac{\mathrm{d}\ln H}{\mathrm{d}z}. \tag{4}$$

We will show below that the first term on the right-hand side, $|\frac{5}{3}\mathrm{d}\ln M_h/\mathrm{d}z|$, is of the order of unity. How about the other terms? We tracked the evolution of the parameter α of haloes in the EAGLE L0100N1504 dark matter-only simulation along their merger tree. The result is plotted in Fig. 2, where different colours refer to haloes in bins of their redshift $z = 0$ mass, $M_{h,0}$. As was the case of the virial ratio, there is clearly some evolution in α as a halo grows, but that evolution is relatively weak and we will neglect it. We also note that the term $(2/3)\mathrm{d}\ln H/\mathrm{d}z$ is always $<1/2$. Therefore, the last two terms in equation (4) are small compared to the first term on the right-hand side, therefore $\mathrm{d}\ln|E_h|/\mathrm{d}z \approx \kappa d\ln M_h/\mathrm{d}z$ with $\kappa \approx 5/3$. To test this approximation in more detail, we once more track haloes along their merger tree to compute $\mathrm{d}\ln|E_h|/\mathrm{d}\ln M_h$ directly (the result is plotted in Fig. 3); different colours refer to haloes in bins of $M_{h,0}$. As M_h increases, $|E_h|$ increases, with $\mathrm{d}\ln|E_h|/\mathrm{d}\ln M_h \approx 5/3$. Combining this approximation with equation (3) motivates us to parametrize the rate of change of energy as a halo grows in mass by

$$\dot{E}_h = -\frac{\kappa}{2}\dot{M}_h {v_h}^2. \tag{5}$$

The variables α (equation 3) and κ are two of the four parameters of the $Ik\epsilon\alpha$ model, and as we just showed, they are approximately independent of halo mass and redshift, and we will simply keep

them constant at $\alpha = 1$ and $\kappa = 5/3$. We proceed by parametrizing the evolution of $M_{\rm h}$.

The increase with time of the halo mass in the extended Press–Schecher (EPS) or 'excursion set' formalism (Bond et al. 1991; Lacey & Cole 1993) describes the growth measured in simulations very well. Here we will use the parametrization described by Correa et al. (2015a) and Correa et al. (2015b), which we write in the form of the value of the halo mass at redshift $z = 0$, $M_{\rm h,0}$, times a dimensionless function $m_{\rm h}(z)$,

$$M_{\rm h} = M_{\rm h,0}\, m_{\rm h}(z)$$

$$m_{\rm h}(z) \approx (1+z)^a \exp(-bz). \tag{6}$$

The corresponding logarithmic growth rate is

$$\frac{{\rm d}\ln M_{\rm h}}{{\rm d}z} = (a-b)\xi_{\rm h}(z)$$

$$\xi_{\rm h}(z) = \frac{1}{a-b}\left(\frac{a}{1+z} - b\right). \tag{7}$$

The dimensionless functions $m_{\rm h}$ and $\xi_{\rm h}(z)$ are both unity at $z = 0$. Since haloes grow in mass, ${\rm d}\ln M_{\rm h}/{\rm d}z \leq 0$, and in terms of the previous equation we have that the function $\xi_{\rm h}(z) > 0$ but $a - b < 0$. The parameters a and b depend on the mass of the halo at some reference redshift, which we take to be $z = 0$. Averaging over halo masses, Correa et al. (2015b) find

$$\bar{a} \approx 0.24\,, \quad \bar{b} \approx 0.75. \tag{8}$$

We will use $\bar{a}$ and $\bar{b}$ and denote them by a and b in our derivations, but in our figures we will use the more elaborate but more accurate version discussed by Correa et al. (2015b) in which a and b are functions of $M_{\rm h,0}$ (except in Figs 5 and 15 in which we use the constant values from equation 8). Using $\bar{a}$ and $\bar{b}$ gives $|(5/3){\rm d}\ln M_{\rm h,0}/{\rm d}z| = 0.85$ at $z = 0$ and 1.25 for $z \to \infty$, therefore $|(5/3){\rm d}\ln M_{\rm h}/{\rm d}z|$ is of the order of unity, as we used before.

The virial velocity's evolution follows from equation (3),

$$v_{\rm h}^2(z) = v_{\rm h,0}^2\, (m_{\rm h}(z)\mathcal{H}(z))^{2/3}\,, \tag{9}$$

where the function $\mathcal{H}(z)$ is defined by

$$\mathcal{H}(z) \equiv \frac{H(z)}{H_0}. \tag{10}$$

2.4 The growth of a galaxy

2.4.1 Stability of feedback-regulated galaxy formation

A (central) galaxy too satisfies the equivalent of equation (5). We neglect any preprocessing of the accreted matter, so that the ratio of gas mass that accretes on to the galaxy to total mass accreted on to the galactic halo is simply the cosmological ratio $\omega_{\rm b}$ of the baryon to the total matter density,

$$\omega_{\rm b} \equiv \frac{\Omega_{\rm b}}{\Omega_{\rm dm} + \Omega_{\rm b}} = \frac{\Omega_{\rm b}}{\Omega_{\rm m}}. \tag{11}$$

Once more, neglecting the effect of the growing galaxy on the dark matter halo leads us to deduce that cosmological accretion decreases the energy of a galaxy at a rate $\dot{E}_{\rm g} = -(\kappa/2)\omega_{\rm b}\dot{M}_{\rm h}{v_{\rm h}}^2$ (subscript 'g' for galaxy).

However, unlike the case of the dark matter halo, the growing galaxy *generates* energy through feedback from stars (and AGN, discussed later), therefore

$$\dot{E}_{\rm g} = \dot{E}_\star - \frac{\kappa}{2}\omega_{\rm b}\,\dot{M}_{\rm h}{v_{\rm h}}^2. \tag{12}$$

In analogy with equation (1), we now speculate that $\dot{E}_\star \approx \frac{\kappa}{2}\omega_{\rm b}\,\dot{M}_{\rm h}{v_{\rm h}}^2$: Feedback from star formation compensates the energy loss associated with cosmological accretion so that the galaxy grows at nearly constant energy. Fig. 4 supports this *ansatz*: It shows that, whereas the energy $E_{\rm h}$ of the dark matter halo (black curve) increases by almost 2 orders of magnitude from a lookback time of 10 Gyr to the present, the energy of the galaxy, $E_{\rm g}$ (blue curve), changes by less than ∼50 per cent over the same time interval.

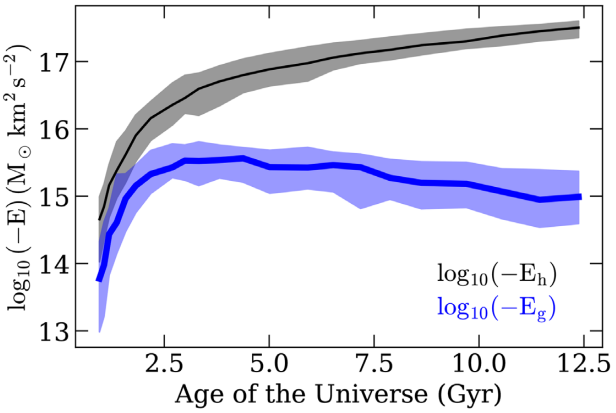

Figure 4. The evolution of the total energy of the dark matter halo, $E_{\rm h}$ (*black*), and the total energy of the star-forming gas, $E_{\rm g}$ (*blue*), along the merger tree of a halo of $z = 0$ mass, $M_{\rm h,\,0} = [0.8\text{–}1.2] \times 10^{13}$ M$_\odot$, selected from the EAGLE simulation Ref-L100N1504. The solid curves show the median relation while the shaded area encompasses the 25–75th percentiles. While the total energy of the dark halo keeps on decreasing, the energy of the central galaxy decreases (secularly) at a slower rate as it is regulated by feedback from star formation.

Most of the energy injected into the galaxy's ISM is associated with star formation (i.e. supernovae and other processes associated with short-lived massive stars), therefore we write $\dot{E}_\star$ in terms of the star formation rate, $\dot{M}_\star$, and a characteristic velocity $v_\star$,

$$\dot{E}_\star = \frac{1}{2}\dot{M}_\star\, v_\star^2. \tag{13}$$

We can obtain an order of magnitude estimate for $v_\star$ by assuming that most of the injected energy is from core-collapse supernovae (SNe), which inject 10^{51} erg of energy each and occur once per $100/\eta$ solar masses worth of stars formed,[2] hence

$$v_\star = \left(\epsilon\eta\frac{2\times10^{51}{\rm erg}}{100\ {\rm M}_\odot}\right)^{1/2}$$

$$\approx 400\left(\frac{\epsilon}{0.091}\times\frac{\eta}{1.74}\right)^{1/2}\ {\rm km\ s^{-1}}. \tag{14}$$

The factor ϵ accounts for radiative losses, with $\epsilon = 1$ corresponding to no radiative losses and $\epsilon \ll 1$ when such losses are substantial. Numerical simulations of SNe going off in a range of gas densities (e.g. Thornton et al. 1998, and reference therein), and analytical models of the wind in M82 combined with simulations (e.g.

[2] $\eta = 1.74$ for a Chabrier (2003) stellar initial mass function that consists of stars in the mass range of [0.1, 100] M$_\odot$, of which those with mass 6–100 M$_\odot$ explode as a core-collapse SN.

Strickland & Heckman 2009), suggest that a large fraction of the injected energy is radiated, $1-\epsilon \approx 90$ per cent. The cooling rate of a radiating plasma also depends on its metallicity, therefore ϵ is unlikely to be constant in all galaxies and at all times. In this paper, we use ϵ as a fitting parameter when comparing to the simulations; we used a reference value of $\epsilon = 0.091$ in equation (14), which is consistent with the expected radiative losses being substantial *and* yields a round number for $v_\star$.

Equation (12) that describes the rate of change of the energy of a galaxy is reminiscent of equation (1) that describes the rate of change of a main-sequence star: Whereas the star loses energy (becomes more bound) through radiative losses, the galaxy becomes more bound as the potential well of its host halo deepens due to cosmological accretion. While the star reacts by compensating the energy loss by nuclear fusion, the galaxy reacts by forming stars that inject energy in the galaxy's star-forming gas. For stars, this results in $\dot{E} = \dot{E}_{\rm nucl} - L = 0$, and we propose here that the same is true for a galaxy, $\dot{E}_{\rm g} = \dot{E}_\star - (\kappa/2)\omega_{\rm b}\dot{M}_{\rm h}{v_{\rm h}}^2 \approx 0$.

Why would the feedback from star formation be just so that $\dot{E}_{\rm g} \approx 0$? Is the equilibrium situation stable in the galaxy's case, just as it was for the star? To examine this question, suppose that $\dot{E}_{\rm g} < 0$, i.e. $|E_{\rm g}|$ is increasing because the galaxy is currently undergoing too little star formation given the current cosmological accretion rate. With gas in the galaxy getting compressed by the deepening potential well, the internal energy $U_{\rm g}$ of the galaxy will increase. How does that affect the star formation rate?

In the EAGLE implementation of star formation, an increase in thermal energy per unit mass implies an increase in pressure, $P \propto u^4$ from equation (A3), and hence an increase in star formation rate, $\dot{\rho}_\star \propto u^{4(n-1)/2} \approx u^{0.8}$ from equation (A1) for $n = 1.4$ from equation (A2). Therefore, an increase in the accretion rate results in an increase in the star formation rate (and conversely, a decrease in the accretion rate results in a decrease in the star formation rate), so that the equilibrium[3] situation, $\dot{E}_{\rm g} = 0$, is secularly stable – just as in the case of nuclear fusion in a main-sequence star, and for a similar reason.[4] We note in particular that the increase in star formation rate due to increased accretion *neither* assumes *nor* requires that the gas mass – the fuel for star formation – increases. In our model, the gas reservoir is *not* regulating the star formation rate in a galaxy. We also note that stability requires that the star formation rate increases with the ISM's pressure, but without requiring any detailed form of the dependence of $\dot{\rho}_\star$ on P: *The details of exactly how star formation feedback operates are unimportant for the secular stability of the star formation rate in a star-forming galaxy*. Another consequence is that the star formation rate in a cosmological galaxy depends very little, if at all, on the star formation law that relates star formation rate to the gas mass.[5]

The star formation rate in our model of feedback-regulated galaxy formation depends on the stellar **I**nitial mass function (through η and the recycle fraction $\mathcal{R}$ discussed below) and the parameters κ (equation 5), ϵ (equation 14), and α (equation 2), which is why we called it $I\kappa\epsilon\alpha$. By computing the star formation rate and stellar mass as a function of halo mass, we next show that $I\kappa\epsilon\alpha$ galaxies lie on a star-forming main sequence.

[3]If the dynamical time-scales are very short, then self-regulation may fail to keep the galaxy in equilibrium. This may happen for example at high redshift (e.g. Duffy et al. 2010)

[4]To take the analogy further, the galaxy in its galactic halo plays the role of the stellar core in the main-sequence star.

[5]We note this is not true in simulations of an *isolated* galaxy, for which the simulator specifies the gas fraction.

2.4.2 *The main sequence of star-forming galaxies*

Setting $\dot{E}_{\rm g} = 0$ in equation (12) for a self-regulating galaxy results in a relation between a galaxy's star formation rate and the cosmological accretion rate on to its host halo at a given redshift,

$$\frac{1}{2}\dot{M}_\star v_\star^2 = \frac{\kappa}{2}\omega_{\rm b}\dot{M}_{\rm h}\,{v_{\rm h}}^2, \tag{15}$$

which is the main result of this paper. The right-hand side is the cosmological *energy* accretion rate on to a halo of a given mass. The left-hand side sets the corresponding star formation rate in the galaxy, in terms of the effective energy injection rate per stellar mass formed. Substituting the expressions for the accretion rate $\dot{M}_{\rm h}$ and virial velocity $v_{\rm h}$ from equations (6) and (9) allows us to write the star formation rate as a product of its value at $z = 0$, $\dot{M}_{\star,0}$, times a dimensionless function, $\Psi_\star(z)$,

$$\begin{aligned}
\dot{M}_\star(z) &= \kappa\omega_{\rm b}\dot{M}_{\rm h}\frac{{v_{\rm h}}^2}{v_\star^2} \equiv \dot{M}_{\star,0}\Psi_\star(z)\\
\dot{M}_{\star,0} &= \kappa\omega_{\rm b}(b-a)H_0 M_{\rm h,0}\frac{v_{\rm h,0}^2}{v_\star^2}\\
&= 1.2\,{\rm M_\odot yr^{-1}}\,\frac{\kappa}{5/3}\,\frac{\alpha}{1}\left[\frac{h}{0.677}\right]^{5/3}\left[\frac{M_{\rm h,0}}{10^{12}\,{\rm M_\odot}}\right]^{5/3}\\
&\quad\times\left[\frac{v_\star}{400\,{\rm km\,s^{-1}}}\right]^{-2}\\
\Psi_\star(z) &= (1+z)\xi_{\rm h}(z)\,(m_{\rm h}(z)\,\mathcal{H}(z))^{5/3}\,.
\end{aligned} \tag{16}$$

The star formation rate scales $\propto M_{\rm h,0}^{5/3} \propto v_{\rm h,0}^5$; the function $\Psi_\star(z = 0) = 1$.

Since stars lose mass during stellar evolution, the time integral of the star formation rate does not equal the total stellar mass at some later time. In the 'instantaneous recycling approximation',

$$M_\star(t) = (1-\mathcal{R})\int_0^t \dot{M}_\star(t')\,{\rm d}t', \tag{17}$$

where $\mathcal{R}$ is the fraction of mass originally in stars that is returned back to star-forming gas through stellar mass-loss; the stellar population models used in EAGLE have $1-\mathcal{R} \approx 0.55$ (Wiersma et al. 2009). The stellar mass is in this approximation

$$\begin{aligned}
M_\star(z) &= (1-\mathcal{R})\frac{\dot{M}_{\star,0}}{H_0}\int_z^\infty \Psi_\star(z')(1+z')^{-1}\mathcal{H}(z')^{-1}\,{\rm d}z'\\
&\equiv M_{\star,0}\,m_\star(z)\\
M_{\star,0} &= (1-\mathcal{R})\frac{\dot{M}_{\star,0}}{H_0}\,m_{\star,0}\\
&= 1.7\times10^{10}\,{\rm M_\odot}\,\frac{1-\mathcal{R}}{0.55}\left[\frac{h}{0.677}\right]^{2/3}\frac{\kappa}{5/3}\,\frac{\alpha}{1}\\
&\quad\times\left[\frac{M_{\rm h,0}}{10^{12}\,{\rm M_\odot}}\right]^{5/3}\left[\frac{v_\star}{400\,{\rm km\,s^{-1}}}\right]^{-2}\\
m_\star(z) &= \frac{1}{m_{\star,0}}\int_z^\infty \Psi_\star(z')(1+z')^{-1}\mathcal{H}(z')^{-1}\,{\rm d}z'\\
m_{\star,0} &= \int_0^\infty \Psi_\star(z')(1+z')^{-1}\mathcal{H}(z')^{-1}\,{\rm d}z' = 1.78,
\end{aligned} \tag{18}$$

with $m_\star(z = 0) = 1$. To evaluate $M_{\star,0}$ and $\dot{M}_{\star,0}$ we have used the cosmological parameters $\Omega_{\rm b} = 0.048\,2519$, $\Omega_{\rm m} = 0.307$, $\Omega_\Lambda = 1-\Omega_{\rm m}$, $\omega_{\rm b} = 0.157$, and $h = 0.677$ from Planck Collaboration I

(2014), and set $a = \bar{a}$ and $b = \bar{b}$ for the redshift dependence of the halo accretion rate from equation (8); numerical values in our figures correspond to the more general accretion histories from Correa et al. (2015b), for which a and b depend on $M_{\rm h,\,0}$.

The specific star formation rate, sSFR, follows from combining equations (16) and (18),

$$\mathrm{sSFR}(z) \equiv \frac{\dot{M}_\star(z)}{M_\star(z)} = \frac{H_0}{m_{\star,0}\,(1-\mathcal{R})}\,\frac{\Psi_\star(z)}{m_\star(z)} = \frac{H_0}{m_{\star,0}(1-\mathcal{R})} \approx 0.07\ \mathrm{Gyr}^{-1} \text{ at } z = 0. \quad (19)$$

This ratio would depend on halo mass and hence also on $M_\star$ if (*i*) we had taken into account that the halo accretion rate depends on halo mass rather than using the average accretion rate from equation (8) and (*ii*) if one or more of the $I\kappa\epsilon\alpha$ parameters were to depend on halo mass.

The expression for the sSFR at $z = 0$ from equation (19) looks suspiciously simple: What sets this numerical value? Tracing back the definitions of the dimensionless functions $\mathcal{H}(z)$ (equation 10), $\Psi_\star(z)$ (equation 16), and $m_\star$ (equation 18), we see that these *only* depend on cosmology and the growth rate of dark matter haloes. Changing the growth rate will change the value of the numerical constant $m_{\star,\,0}$ in equation (18). The only other $I\kappa\epsilon\alpha$ parameter that sets the sSFR is $\mathcal{R}$, the recycled mass fraction, which depends on the IMF. Therefore, the value of the sSFR at $z = 0$ depends on cosmology (through the accretion history of haloes), and on the fraction of mass returned to the ISM during stellar evolution, $\mathcal{R}$, and nothing else. This is of course a consequence of assuming that none of the $I\kappa\epsilon\alpha$ parameters evolve.

The dimensionless functions $\Psi_\star(z)$, $m_\star(z)$, and $\Psi_\star(z)/m_\star(z)$ provide the unique connection between the stellar properties of a galaxy and the properties of its host halo; they are plotted in Fig. 5. The star formation rate of an $I\kappa\epsilon\alpha$ galaxy varies over a factor of $\sim$6 between $z = 0$ and 6, peaking at $z \sim 2$, with half the stellar mass forming below $z \sim 1$. The sSFR increases rapidly with redshift, and is higher than its $z = 0$ value by factors of 4.6, 13.7, and 30 at redshifts 1, 2, and 3, respectively.

To summarize: $I\kappa\epsilon\alpha$ predicts a main sequence of star-forming galaxies along which the sSFR does not depend on $M_\star$, provided the $I\kappa\epsilon\alpha$ parameters themselves do not depend on halo mass. The value of this sSFR increases rapidly with redshift.

2.4.3 *Comparison to* EAGLE

We test the ideas put forward in the previous section by comparing the star formation rate of galaxies as a function of halo properties and redshift to that of EAGLE galaxies. We emphasize that for a given assumed stellar IMF, the ϵ parameter of the $I\kappa\epsilon\alpha$ model – a measure of the radiative losses in the ISM of the energy injected by SNe – is the central free parameter that sets the star formation rate in a cosmological halo. It does so by setting the characteristic velocity $v_\star$ through equation (14). The parameter ϵ likely depends on the properties of a galaxy's ISM – presumably ϵ would be smaller (greater cooling losses) when the ISM is denser and more metal rich. Rather than proposing a more detailed model for this, at this stage we simply keep ϵ constant. However, the EAGLE reference simulation has a parameter $f_{\rm th}$ that explicitly changes the amount of energy injected into the ISM per solar mass of stars formed, depending on density and metallicity of the ISM (see equation 7 in Schaye et al. 2015). Therefore, to keep the comparison between $I\kappa\epsilon\alpha$ and EAGLE fair, we compare here to the 'FBconstnoAGN' EAGLE variation, in which $f_{\rm th}$ is kept constant (and which does not include AGN feedback either; see the appendix for more details). We reiterate though, that keeping $f_{\rm th}$ constant is not quite equivalent to keeping ϵ constant, because the cooling losses in EAGLE still depend on density and metallicity.

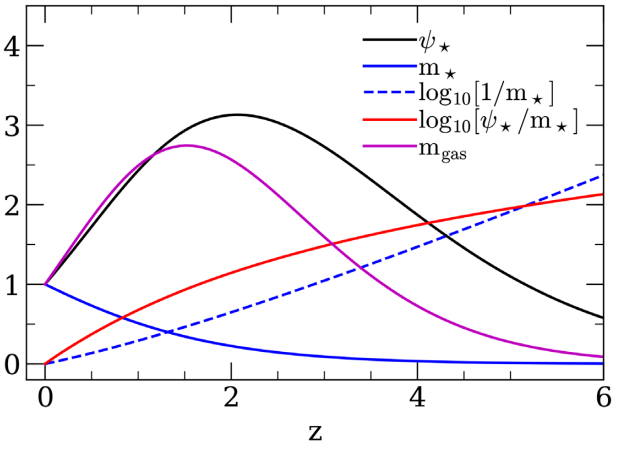

Figure 5. The evolution of the dimensionless star formation rate $\Psi_\star(z)$ (black curve) from equation (16), stellar mass $m_\star(z)$ (blue curve; we also plot $\log_{10} 1/m_\star$ as a dashed blue line) from equation (18), sSFR $\Psi_\star(z)/m_\star(z)$ (red curve) from equation (19), and the gas mass $m_{\rm gas}$ (magenta curve) from equation (29). We used $a = \bar{a}$ and $b = \bar{b}$ for the accretion history of haloes (equation 7).

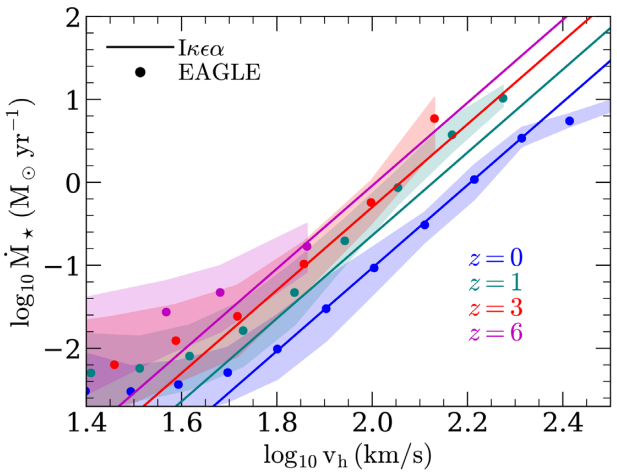

Figure 6. The dependence of the star formation rate, $\dot{M}_\star$, on the virial velocity $v_{\rm h}$ of a galaxy's host halo, at different redshifts. The *coloured lines* are the predictions from the $I\kappa\epsilon\alpha$ model (equation 16, with $\epsilon = 0.2$) based on our self-regulation arguments; the *large dots* are the median star formation rate in EAGLE galaxies (simulation FBconstnoAGN), with the *shaded area* encompassing the 25–75th percentile range. Different colours correspond to different redshifts (*blue, green, red, and purple* correspond to $z = 0$, 1, 3, and 6, respectively). The $I\kappa\epsilon\alpha$ model captures well the dependence of $\dot{M}_\star$ on $v_{\rm h}$ and z.

The star formation rate predicted by equation (16) is compared to the EAGLE FBconstnoAGN model in Fig. 6, taking $\alpha = 1$, $\kappa = 5/3$, $\eta = 1.7$, and $\epsilon = 0.2$ (so that $v_\star$ is constant; see equation 14); the coloured lines are the $I\kappa\epsilon\alpha$ prediction at different redshifts, and the large dots are the median relation for EAGLE galaxies with the shaded region encompassing the 25–75th percentile range. Even when keeping $v_\star$ constant, equation (16) captures accurately the increase in $\dot{M}_\star$ with the halo's virial velocity $v_{\rm h}$ at fixed z, as well

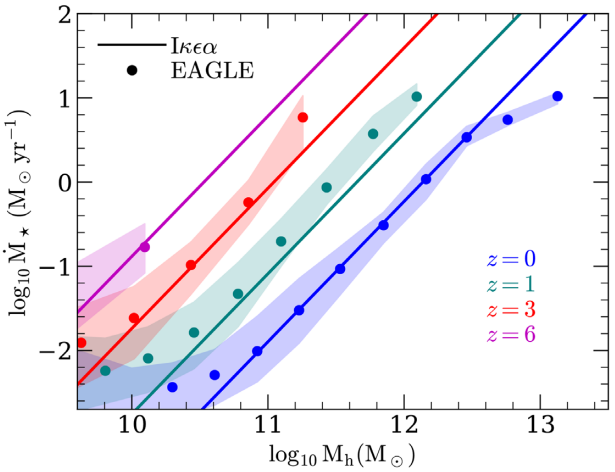

Figure 7. Same as Fig. 6, but for the dependence of $\dot{M}_\star$ on halo mass, M_h.

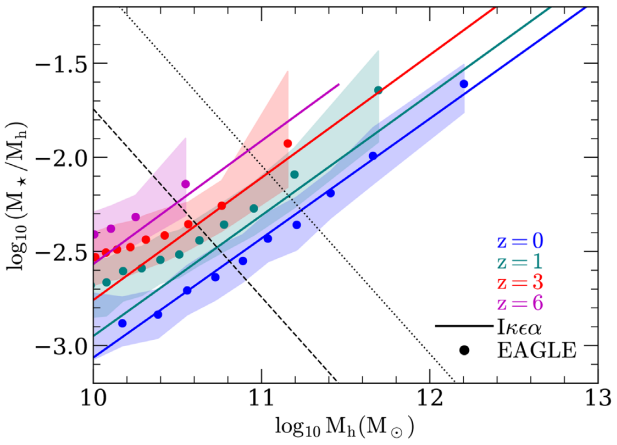

Figure 8. The stellar mass–halo mass ratio, $M_\star/M_\mathrm{h}$, as a function of M_h at different redshifts. The *coloured lines* are the predictions from the $I\kappa\epsilon\alpha$ model ($M_\star$ from equation 18); the *large dots* are the median relation in the EAGLE galaxies (simulation FbconstnoAGN), with the *shaded area* encompassing the 25–75th percentile range. Different colours correspond to different redshifts (*blue, green, red, and purple* correspond to $z = 0$, 1, 3, and 6, respectively). The *black dashed* and *black dotted* lines correspond to EAGLE galaxies with approximately 100 and 500 star particles, respectively.

as the increase in $\dot{M}_\star$ with z at fixed v_h. With only one 'free' model parameter ϵ (which sets $v_\star$), we were astonished by the level of agreement between $I\kappa\epsilon\alpha$ and EAGLE.

In the case of Fig. 6, the increase in $\dot{M}_\star$ with z at given v_h is due to the increase in the cosmological accretion rate on to a halo with given v_h at given z, as is apparent from equation (15). However, plotting $\dot{M}_\star$ as a function of M_h (Fig. 7), we see that the redshift dependence is stronger due to the $\mathcal{H}(z)^{2/3}$ dependence of equation (16). This is not surprising within the context of our self-regulation model: the star formation rate depends on virial velocity rather than halo mass.

2.5 The $M_\star$–M_h relation

The stellar mass of a galaxy in equation (18) is the product of a dimensional number that depends on the galaxy's halo mass at $z = 0$, $M_{\mathrm{h},0}$, times a dimensionless function $m_\star(z)$. This functional dependence allows us to answer the question of 'what is the $M_\star$–M_h relation in $I\kappa\epsilon\alpha$' in two different ways: (*i*) 'What is the $M_\star$–M_h relation for a population of galaxies at a given redshift?', and (*ii*) 'How does the $M_\star$–M_h ratio of a halo evolve?' The answer to the first question follows from $M_\star \propto M_{\mathrm{h},0}^{5/3}$ and $M_\mathrm{h} \propto M_{\mathrm{h},0}$, therefore

$$\frac{\mathrm{d}\ln M_\star}{\mathrm{d}\ln M_\mathrm{h}}|_{z=\mathrm{const}} = \frac{5}{3}. \tag{20}$$

The value of the exponent can be traced back to the $\dot{M}_\mathrm{h}\, {v_\mathrm{h}}^2 \propto {M_\mathrm{h}}^{5/3}$ dependence of the star formation rate on halo mass (equation 16). We compare the predicted relation to that measured in EAGLE in Fig. 8: The coloured lines are the theoretical predictions at different redshifts, and the large dots are the median relation for EAGLE galaxies with the shaded region encompassing the 25–75th percentile range. Given that $I\kappa\epsilon\alpha$ predicts the dependence of $\dot{M}_\star$ on M_h as a function of z in EAGLE variation FBconstnoAGN well, it is not very surprising that it also reproduces the relation between $M_\star$ and M_h.

Although $I\kappa\epsilon\alpha$ galaxies lie along a line with $M_\star/M_\mathrm{h} \propto {M_\mathrm{h}}^{2/3}$, they do not evolve along this line. The $M_\star$–M_h ratio for a given halo evolves as

$$\frac{\mathrm{d}\ln M_\star}{\mathrm{d}\ln M_\mathrm{h}}|_{M_{\mathrm{h},0}=\mathrm{const}} = -\frac{m_\mathrm{h}(z)}{m_{\star,0}(a-b)m_\star(z)}(m_\mathrm{h}(z)\mathcal{H}(z))^{2/3}. \tag{21}$$

This logarithmic slope is ≈1.1 at $z = 0$ and increases with z to become nearly constant at a value of 1.4 for $z \geq 4$. If this slope were 5/3, then (star-forming) galaxies would evolve along the $z = 0$ $M_\star$–M_h relation so that the stellar mass in a halo of a given mass would be independent of redshift. Because the slope is less than 5/3, the $M_\star/M_\mathrm{h}$ versus M_h relation evolves with redshift, in the sense that the stellar mass increases with redshift at a constant halo mass; however, that evolution is not very strong. This is the redshift evolution seen in Fig. 8.

Summarizing, we conclude that $I\kappa\epsilon\alpha$ reproduces the relation between halo mass, star formation rate, and stellar mass measured in the FBconstnoAGN EAGLE variation. The fact that $I\kappa\epsilon\alpha$ reproduces the dependence of $\dot{M}_\star$ on M_h is particularly encouraging, since it directly tests the very basis of the self-regulation argument of equation (15). Interestingly, the star formation rate predicted by equation (16) does not depend *at all* on the galaxy's gas mass or indeed the assumed star formation law – as long as $\dot{\rho}_\star \propto u^\zeta$ for some sufficiently large and positive value of the exponent ζ, so that the star formation rate *increases* with the pressure of the galaxy's ISM. Instead, the star formation rate depends on the cosmological accretion rate, and on $v_\star$ – that is, on the efficiency of stellar feedback. We will return to this point in the discussion section.

2.6 The GSMF

We compute the GSMF by combining the $M_\star$–M_h relation from $I\kappa\epsilon\alpha$ with a model for the evolution of the halo-mass function. The Press–Schechter (PS; Press & Schechter 1974) approximation for the actual number density of haloes per dex in halo mass (e.g. Reed et al. 2007), at $z = 0$, is

$$\frac{\mathrm{d}n_\mathrm{h}}{\mathrm{d}\log M_{\mathrm{h},0}} = n_0 \left(\frac{M_{\mathrm{h},0}}{M_\mathrm{ps}}\right)^{-\alpha_\mathrm{h}} \exp\left(-\frac{M_{\mathrm{h},0}}{M_\mathrm{ps}}\right), \tag{22}$$

where $n_0 \approx 1 \times 10^{-4}\,\mathrm{Mpc}^{-3}$ is a normalization constant, $M_\mathrm{ps} \approx 2 \times 10^{14}\,\mathrm{M}_\odot$ a characteristic mass above which the number density of haloes falls exponentially, and the exponent $\alpha_\mathrm{h} \approx 0.9$. In the approximation that all haloes grow at the same logarithmic rate,

$M_{\rm h}(z) = M_{\rm h,0}\, m_{\rm h}(z)$, the halo-mass function at redshift z is

$$\frac{{\rm d}n_{\rm h}}{{\rm d}\log M_{\rm h}} = n_0 \left(\frac{M_{\rm h}}{m_{\rm h}(z)\, M_{\rm ps}}\right)^{-\alpha_{\rm h}} \exp\left(-\frac{M_{\rm h}}{m_{\rm h}(z) M_{\rm ps}}\right), \tag{23}$$

where n_0 and $M_{\rm PS}$ are redshift independent, and $n_{\rm h}$ is now the comoving number density of haloes per dex in halo mass. Provided the $I\kappa\epsilon\alpha$ parameters are constants, $M_\star \propto {M_{\rm h}}^{5/3}$, and the comoving number density of galaxies per dex in stellar mass becomes

$$\begin{aligned}
\frac{{\rm d}n_{\rm g}}{{\rm d}\log M_\star} &= \frac{3n_0}{5}\left(\frac{M_\star}{m_\star(z) M_{\star,\rm ps}}\right)^{-\alpha_\star} \exp\left(-\frac{M_\star}{m_\star(z) M_{\star,\rm ps}}\right)\\
M_{\star,\rm ps} &= M_{\star,0}\left(\frac{M_{\rm ps}}{10^{12}{\rm M}_\odot}\right)^{5/3}\\
&\approx 1.7\times 10^{10}\left(\frac{M_{\rm ps}}{10^{12}{\rm M}_\odot}\right)^{5/3}{\rm M}_\odot\\
\alpha_\star &= \frac{3}{5}\alpha_{\rm h} \approx 0.54.
\end{aligned} \tag{24}$$

In this approximation, the GSMF is just a scaled version of the halo-mass function, with a power-law shape at low masses and an exponential cut-off at high masses. However, it is well known that the 'knee' in the GSMF – above which the exponential sets in – does not correspond to the knee in the halo-mass function, but rather is a consequence of AGN feedback (Bower et al. 2006; Croton et al. 2006). We discuss how this can be incorporated in the model in Section 3.4 below.

It is interesting to note that we can make the same argument that leads to equation (24) to the star formation rate of a galaxy and compute the 'galaxy star formation rate function', GSRF, the number density of galaxies per dex of star formation rate. Since $\dot{M}_\star \propto {M_{\rm h}}^{5/3}$, the GSRF has the same shape as the GSMF,

$$\begin{aligned}
\frac{{\rm d}n_{\rm g}}{{\rm d}\log \dot{M}_\star} &= \frac{3n_0}{5}\left(\frac{\dot{M}_\star}{\Psi_\star(z)\dot{M}_{\star,\rm ps}}\right)^{-\alpha_\star} \exp\left(-\frac{\dot{M}_\star}{\Psi_\star(z)\dot{M}_{\star,\rm ps}}\right)\\
\dot{M}_{\star,\rm ps} &= \dot{M}_{\star,0}\left(\frac{M_{\rm ps}}{10^{12}{\rm M}_\odot}\right)^{5/3}\\
&\approx 1.2\left(\frac{M_{\rm ps}}{10^{12}{\rm M}_\odot}\right)^{5/3}{\rm M}_\odot\ {\rm yr}^{-1}.
\end{aligned} \tag{25}$$

The constants $\dot{M}_{\star,0}(M_{\rm h,0} = 10^{12}\,{\rm M}_\odot, z=0)$ and $M_{\star,0}(M_{\rm h,0} = 10^{12}\,{\rm M}_\odot, z=0)$ are the $z=0$ star formation rate and stellar mass of a galaxy in a halo of mass $10^{12}\,{\rm M}_\odot$; the numerical values for these are taken from equations (16) and (18), respectively.

At sufficiently low halo mass, these functions are power laws with a slope $3\alpha_{\rm h}/5 \approx 0.54$. The comoving number density of galaxies with a given stellar mass increases monotonically with decreasing redshift $\propto m_\star(z)^{\alpha_\star}$. The corresponding evolution of the comoving number density of galaxies with a given star formation rate is $\propto \Psi_\star(z)^{\alpha_\star}$: This function is not monotonic but peaks around $z\sim 2$. It falls to approximately 0.5 and 0.54 times its $z=2$ value at redshifts $z=5.5$ and 0, respectively.

The $I\kappa\epsilon\alpha$ star formation in a halo with low $v_{\rm h}$ is much less than the rate at which that halo accretes gas. Indeed, according to equation (15), only a fraction $\kappa {v_{\rm h}}^2/v_\star^2$ of the accreted gas goes into stars. What happens to the remaining gas? Also, self-regulation due to feedback from star formation must eventually fail for sufficiently high values of $v_{\rm h} \approx v_\star/\kappa^{1/2} \approx 310$ km s^{-1}, since then the star formation rate required to self-regulate would *exceed* the gas accretion rate. To investigate the consequence of these considerations in more detail, we next examine the gas properties in $I\kappa\epsilon\alpha$.

3 GALACTIC WINDS AND THE FAILURE OF SELF-REGULATING STELLAR FEEDBACK

3.1 Galaxy sizes and gas fractions

The star formation rate in the $I\kappa\epsilon\alpha$ model does not depend on the gas mass. Instead, we *compute* the mass of star-forming gas by assuming a star formation law. Taking the Kennicutt–Schmidt (Kennicutt 1998) star formation law and assuming that star-forming gas is in an exponential disc with scale length $R_{\rm gas}$, the (total) star formation rate of a galaxy is related to its gas mass by

$$\dot{M}_\star = \frac{2\pi A\, R_{\rm gas}^2}{n^2}\left(\frac{M_{\rm gas}/{\rm M}_\odot}{2\pi({R_{\rm gas}}/{\rm pc})^2}\right)^n, \tag{26}$$

where A and n are the parameters of the Kennicutt–Schmidt law (equation A2). We follow Mo et al. (1998) (see also Kravtsov 2013) by assuming[6] that disc size, $R_{\rm gas}$, is a constant fraction, λ, of the halo's virial radius. Using equation (2), this yields

$$\begin{aligned}
R_{\rm gas} &= \lambda\, R_{\rm h} = R_{\rm gas,0}\, r_{\rm gas}(z)\\
R_{\rm gas,0} &= 2\ {\rm kpc}\ \frac{\lambda}{0.01}\left(\frac{M_{\rm h,0}}{10^{12}{\rm M}_\odot}\right)^{1/3}\\
r_{\rm gas}(z) &= \frac{m_{\rm h}(z)^{1/3}}{\mathcal{H}(z)^{2/3}},
\end{aligned} \tag{27}$$

where $\lambda = 0.01$ yields a reasonable reference scale length of $R_{\rm gas,\,0} = 2$ kpc for the galaxy inhabiting a $10^{12}\,{\rm M}_\odot$ halo at $z=0$. Using the $\dot{M}_\star$–$M_{\rm h,0}$ relation from equation (16) and the $M_\star$–$M_{\rm h,\,0}$ relation from equation (18) allows us to relate galaxy size to star formation rate and stellar mass,

$$\begin{aligned}
\frac{R_{\rm gas}(z)}{2\ {\rm kpc}}\frac{0.01}{\lambda} &= \left(\frac{\dot{M}_\star}{1.2\ {\rm M}_\odot\ {\rm yr}^{-1}}\right)^{1/5}\frac{r_{\rm gas}(z)}{\Psi_\star(z)^{1/5}}\\
&= \left(\frac{M_\star}{1.7\times 10^{10}\ {\rm M}_\odot}\right)^{1/5}\frac{r_{\rm gas}(z)}{m_\star(z)^{1/5}}.
\end{aligned} \tag{28}$$

Sizes of galaxies with a given $M_\star$ depend on redshift $\propto m_{\rm h}^{1/3}/(\mathcal{H}^{2/3} m_\star^{1/5})$. The ratio $m_{\rm h}^{1/3}/m_\star^{1/5}$ varies by less than a factor of 0.75 below $z=6$, meaning that the size scales approximately as $1/\mathcal{H}(z)^{2/3} = 1/(1+z)$ for $z \gg 1$, and slower than that at lower z. This agrees rather well with the observed scaling: Allen et al. (2017) quote a scaling $\propto (1+z)^{-0.97}$ for redshifts 5–7 and van der Wel et al. (2014) quote a scaling $(1+z)^{-0.75}$ for redshifts 0–3. At a given value of $\dot{M}_\star$, $R_{\rm gas} \propto (1+z)^{-1.7}$ for $z \gg 1$, which is steeper than the $(1+z)^{-1.1}$ quoted by Shibuya, Ouchi & Harikane (2015). The weak dependence of size on mass, $R_{\rm gas} \propto M_\star^{1/5}$, is consistent with the scaling $R_\star \propto M_\star^{0.22}$ for the stellar size–$M_\star$ relation found by van der Wel et al. (2014).

Substituting equation (27) into equation (26) yields

$$\begin{aligned}
M_{\rm gas} &= M_{\rm gas,0}\, m_{\rm gas}(z)\\
\left[\frac{M_{\rm gas,0}}{2.45\times 10^9\ {\rm M}_\odot}\right]^n &= \frac{\kappa}{5/3}\frac{\alpha}{1}\left[\frac{h}{0.677}\right]^{5/3}\left[\frac{\lambda}{0.01}\right]^{2n-2}\\
&\quad\times\left[\frac{v_\star}{400\ {\rm km\ s}^{-1}}\right]^{-2}\left[\frac{M_{\rm h,0}}{10^{12}\ {\rm M}_\odot}\right]^{1+2n/3}\\
m_{\rm gas}(z) &= [\Psi_\star(z)]^{1/n}\,[r_{\rm gas}(z)]^{2-2/n}.
\end{aligned} \tag{29}$$

[6]Mo et al. (1998) apply this reasoning to the stellar disc; Navarro et al. (2017) show that $R_{\rm gas}$ scales better with the scale radius of the halo, but since we neglect variations in halo concentration by taking $\alpha = 1$, these are equivalent.

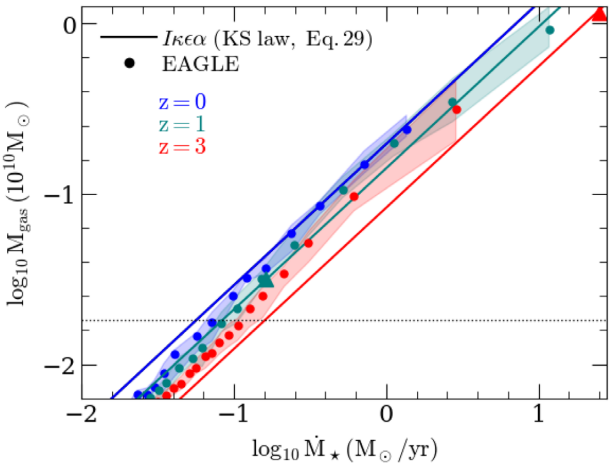

Figure 9. The mass of star-forming gas in galaxies, $M_{\rm gas}$, versus the star formation rate, $\dot{M}_\star$, at different redshifts: $z = 0$ (blue), 1 (green), and 3 (red). The *thick solid lines* show the scaling in $I\kappa\epsilon\alpha$ obtained by using the Kennicut–Schmidt law (equation 26), with $n = 1.4$ and assuming that the scale length of the gas disc evolves as in equation (27) (Mo, Mao & White 1998). The *large coloured dots* are the median relation in the EAGLE galaxies (simulation FbconstnoAGN), with the *shaded regions* encompassing the 25–75th percentile range. The *dotted horizontal line* corresponds to EAGLE galaxies with 100 gas particles. The galaxies for which $R_{\rm gas}$ is less than the gravitational softening length in EAGLE lie below the triangles on each line, indicating that those galaxies are not well resolved in the EAGLE simulation. In the $I\kappa\epsilon\alpha$ model, the amount of gas in the ISM is set by the star formation rate rather than the other way around.

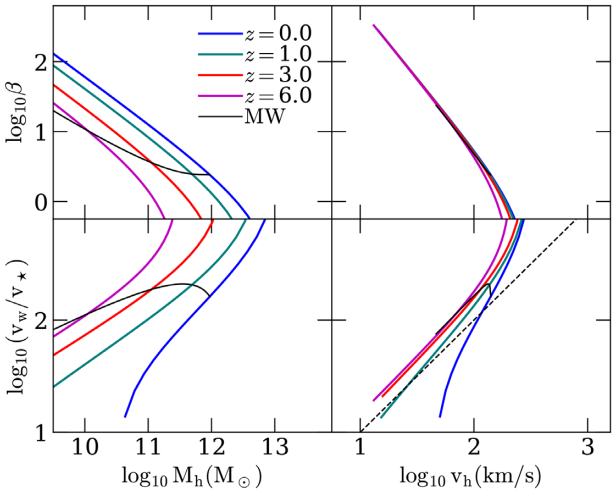

Figure 10. The dependence of the wind mass-loading factor β (*top panels*, from equation 30) and the wind-speed, $v_{\rm w}$, at 5 times the wind launching radius (*bottom panels*, from equation 33) as a function of halo mass, $M_{\rm h}$ (*left-hand panels*), and halo virial velocity, $v_{\rm h}$ (*right-hand panels*), from the $I\kappa\epsilon\alpha$ model. The launching radius of the wind is taken to be equal to the gas scale radius, $R_{\rm gas}$ (equation 27). The coloured lines correspond to $\epsilon = 0.1$, $\kappa = 5/3$, $\alpha = 1$, and $1 - \mathcal{R} = 0.55$ in the $I\kappa\epsilon\alpha$ model, at different redshifts (*blue, green, red, and purple* corresponding to $z = 0$, 1, 3, and 6, respectively). The redshift dependence is stronger as a function of $M_{\rm h}$ than as a function of $v_{\rm h}$. At low values of $v_{\rm h} \lessapprox 120$ km s^{-1}, the wind speed tracks $v_{\rm h}$, and the mass loading decreases from $\beta \sim 30$ at $v_{\rm h} \sim 50$ km s^{-1} to $\beta \sim 1$ at $v_{\rm h} \sim 100$ km s^{-1}. The outflow begins to stall, $\beta \to 0$, for $v_{\rm h} \to 180$ km s^{-1}, at which point the wind speed becomes large, $\sim 10^3$ km s^{-1}. The *black dashed line* in the bottom right-hand panel is the one-to-one relation. The *thin black curve* labelled 'MW' shows the evolution of β and $v_{\rm w}$ for a Milky Way-like galaxy, $z = 0$ halo mass of $M_{\rm h,\,0} = 10^{12}\,{\rm M}_\odot$, as it grows in mass.

Using the $\dot{M}_\star$–$M_{\rm h,0}$ relation from equation (16) allows us to compute the $M_{\rm gas}$–$\dot{M}_\star$ relation, and the result is compared to the EAGLE simulation in Fig. 9, where we used the values of A and n from Kennicutt (1998). The $I\kappa\epsilon\alpha$ prediction reproduces very well the slope of the relation and the normalization at $z = 0$. The simulated evolution is somewhat weaker than predicted. Although pleasing, the excellent agreement between the theoretical prediction and the simulation is not surprising: Galaxies in EAGLE follow the Kennicutt–Schmidt relation of equation (A2), and that relation results in galaxies following equation (26) at least approximately.

The evolution of the gas mass, as governed by the dimensionless function $m_{\rm gas}(z)$ from equation (29), is plotted in Fig. 5. The ratio of $m_{\rm gas}(z)$ over its value at $z = 0$ is 0.5, 0.8, 1.2, and 1.4 at $z = 4$, 3, 2, and 1, respectively, meaning that the gas mass of a forming galaxy changes by slightly more than a factor of 2 since $z = 4$. Therefore, assuming that galaxies form stars at nearly constant gas mass is a relatively good approximation below $z \sim 4$; it forms the basis of the equilibrium model of Davé et al. (2012); see also Bouché et al. (2010) and Krumholz & Dekel (2012).

3.2 Galactic winds

Galactic winds are a natural outcome of a model in which cosmological accretion sets the star formation rate but a star formation law sets the gas mass. Indeed, conservation of baryon mass requires that

$$\omega_{\rm b}\dot{M}_{\rm h} = \dot{M}_{\rm gas} + (1-\mathcal{R})\dot{M}_\star + \dot{M}_{\rm w} \equiv \dot{M}_{\rm gas} + (1+\beta-\mathcal{R})\,\dot{M}_\star, \quad (30)$$

where $\dot{M}_{\rm w}$ is the rate at which the galaxy loses mass through a galactic wind, and the ratio $\beta \equiv \dot{M}_{\rm w}/\dot{M}_\star$ is usually called the 'mass-loading factor' of the wind. Solving for β gives

$$\beta = \frac{v_\star^2}{\kappa {v_{\rm h}}^2} - (1-\mathcal{R}) - \frac{\dot{M}_{\rm gas}}{\dot{M}_\star}, \quad (31)$$

where we used the main $I\kappa\epsilon\alpha$ relation of equation (15) to relate $\dot{M}_\star$ and $\dot{M}_{\rm h}$. We can compute β as a function of redshift and $v_{\rm h}$ or halo mass by integrating this equation using the relation between the gas mass and $\dot{M}_\star$ (equation 26); the result is shown in Figs 10 and 11. The velocity of the outflow can be estimated by assuming that the wind conserves energy once launched,[7]

$$\frac{1}{2}\dot{M}_\star v_\star^2 = \frac{1}{2}\dot{M}_{\rm w}\left(1 + \frac{2}{\mathcal{M}^2\gamma(\gamma-1)}\right)v_{\rm w}^2 + \frac{1}{2}\dot{M}_{\rm w}v_\phi^2$$
$$\frac{1}{2}v_\phi^2 = \frac{c v_{\rm h}^2}{\ln(1+c) - \frac{c}{1+c}}\left[\frac{\ln(1+\frac{cR_{\rm L}}{R_{\rm h}})}{\frac{cR_{\rm L}}{R_{\rm h}}} - \frac{\ln(1+\frac{cR}{R_{\rm h}})}{\frac{cR}{R_{\rm h}}}\right]. \quad (32)$$

$\mathcal{M} = v_{\rm w}/c_{\rm s}$ is the wind's Mach number, $\gamma = 5/3$ is the adiabatic index, $v_\phi^2/2$ is the change in potential of a Navarro–Frenk–White (NFW) halo (Navarro et al. 1997) between the launch cite, $R_{\rm L}$, and the location R where it is measured (e.g. Łokas & Mamon 2001), c is the halo's concentration parameter that depends on $M_{\rm h}$ and z (e.g. Ludlow et al. 2014) and we assume the launch radius, $R_{\rm L} = R_{\rm gas}$. $v_\phi \approx 0$ if the wind speed is measured very close to the launch site, and v_ϕ equals the escape speed from the halo if the wind speed is

[7]This assumption may not be unreasonable because ϵ already accounts significant radiative losses before the wind is launched.

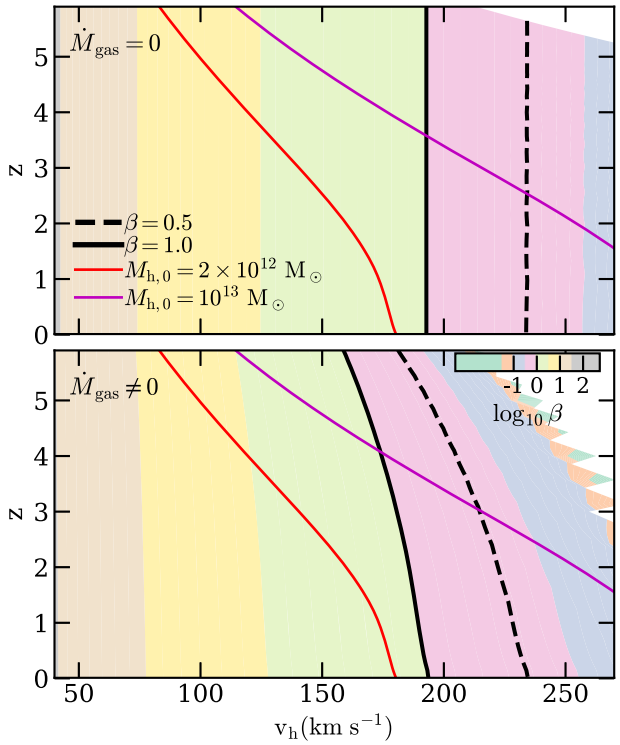

Figure 11. The mass-loading factor β from equation (31) as a function of the halo virial velocity, $v_{\rm h}$, and redshift, z, shown as a colour map, for $\dot{M}_{\rm gas} = 0$ (*top panel*) and for $\dot{M}_{\rm gas} \neq 0$ (*bottom panel*). The dashed and solid black lines correspond to $\beta = 0.5$ and 1, respectively. The red and magenta lines show the evolutionary tracks of two haloes with masses, $M_{\rm h,0} = 2\times10^{12}$ M$_\odot$ and 10^{13} M$_\odot$, respectively.

measured at infinity. This expression also neglects any ram pressure the outflow may suffer. If the outflow is cold, $\mathcal{M} \to \infty$, and

$$v_{\rm w}^2 \approx \frac{v_\star^2}{\beta} - v_\phi^2. \tag{33}$$

Clearly, this treatment of the wind is quite approximate and in particular it is not obvious how one should compare our value of $v_{\rm w}$ to observations, in which the wind speed is often expressed in terms of the full width half-maximum of an emission line. Fortunately, the behaviour of the mass-loading β is independent of these considerations, although here it is not so clear whether β refers to gas leaving the galaxy or gas leaving the halo.

Given these limitations, we plot β, and the wind speed, $v_{\rm w}$, at a distance of 5 times the gas scale radius, $R_{\rm gas}$, as a function of halo mass, virial velocity, and redshift in Fig. 10. The β–$M_{\rm h}$ relation evolves with redshift, as is clear from the left-hand panels of the figure, basically because the relation between $\dot{M}_\star$ and $\dot{M}_{\rm h}$ depends on virial velocity according to equation (15). Most of that redshift dependence is removed if we plot β as a function of $v_{\rm h}$, as is seen from the right-hand panels in the figure. As $v_{\rm h}$ increases, β decreases and $v_{\rm w}$ increases. Also notice that as $v_{\rm h}$ tends to a critical value of around $v_{\rm h,c} \approx 180$ km s^{-1}, β drops precipitously whereas the wind speed *increases* rapidly.

Winds in low-$v_{\rm h}$ galaxies are slow and strongly mass loaded, $\beta \gg 1$, as can be seen from Fig. 10 and 11. When $\beta \gg 1$ and making the further approximation that $|\dot{M}_{\rm gas}| \ll \dot{M}_\star$, equations (30) and (33) combine to

$$v_{\rm w} = \left(\frac{\kappa(1+\beta-\mathcal{R})}{\beta}\right)^{1/2} v_{\rm h} \approx \kappa^{1/2}\, v_{\rm h}. \tag{34}$$

Therefore, the wind speed tracks the halo's virial velocity (in low-$v_{\rm h}$ galaxies at $z < 4$), as is apparent from Fig. 10.

The relation between gas mass and star formation rate that results from the Kennicutt–Schmidt star formation law, equation (29), and the equation for the mass loading of winds, equation (31), have interesting consequences, namely (*i*) the emergence of a mass–metallicity relation, and (*ii*) the existence of a characteristic value of $v_{\rm h}$ above which self-regulation due to feedback from stars fails. We investigate these next.

3.3 The mass–metallicity relation

The metal mass of the star-forming gas, $M_Z \equiv Z\,M_{\rm gas}$, changes due to metals synthesized and released by stars, metals accreted, metals lost in a galactic wind, and metals locked-up in long-lived stars. Its rate of change is therefore

$$\begin{aligned}\dot{M}_Z &= \frac{\rm d}{{\rm d}t}(Z M_{\rm gas}) \\ &= y\dot{M}_\star + Z_0\omega_{\rm b}\dot{M}_{\rm h} - Z_{\rm w}\dot{M}_{\rm w} - Z(1-\mathcal{R})\dot{M}_\star,\end{aligned} \tag{35}$$

where y is the stellar yield, Z_0 is the metallicity of accreted gas, and $Z_{\rm w}$ is the metallicity of the wind that may differ from that of the gas, for example because enriched gas is more like to be ejected by feedback (see e.g. Creasey, Theuns & Bower 2015). Combining this relation with equation (30), which expresses baryon mass conservation, and the main $I\kappa\epsilon\alpha$ relation between $\dot{M}_{\rm h}$ and $\dot{M}_\star$ from equation (15), we find that provided $Z_{\rm w} = Z$ and $Z_0 = 0$,

$$\begin{aligned}\dot{Z} &= y\frac{\dot{M}_\star}{M_{\rm gas}} - Z\frac{\omega_{\rm b}\dot{M}_{\rm h}}{M_{\rm gas}}, \\ &= \frac{\dot{M}_\star}{M_{\rm gas}}\left(y - Z\frac{v_\star^2}{\kappa v_{\rm h}^2}\right).\end{aligned} \tag{36}$$

The recycled fraction $\mathcal{R}$ does not affect $\dot{Z}$ in the instantaneous recycling approximation, and the wind's mass-loading β does not affect $\dot{Z}$ provided $Z_{\rm w} = Z$. Integrating this equation in time, we compare the relation between Z and $v_{\rm h}$ as a function of redshift to the results from EAGLE (simulation FbConstnoAGN) in Fig. 12; the agreement is quite good, with $I\kappa\epsilon\alpha$ showing a somewhat steeper dependence of Z on $M_{\rm h}$ and a lower normalization at Milky Way-like values of $v_{\rm h} \sim 140$ km s^{-1}.

Interestingly though, both $I\kappa\epsilon\alpha$ and EAGLE show very little evolution of the Z–$v_{\rm h}$ relation in Fig. 12. Indeed, equation (36) shows that the metallicity of a galaxy tends to a value $Z \approx \kappa y {v_{\rm h}}^2/v_\star^2$ that in fact only depends on a halo's virial velocity and not explicitly on redshift. In this approximation, the metallicity of a galaxy changes only secularly, tracking the evolution of ${v_{\rm h}}^2$. Such a behaviour is an attractor of equation (36): given that $\dot{M}_\star/M_{\rm gas} > 0$, $\dot{Z}$ is positive (negative) when $Z < y\kappa v_{\rm h}^2/v_\star^2$ (when $Z > y\kappa v_{\rm h}^2/v_\star^2$). Therefore, Z approaches the secular value,

$$Z = \kappa y \frac{v_{\rm h}^2}{v_\star^2}, \tag{37}$$

on the gas consumption time-scale, $M_{\rm gas}/\dot{M}_\star$. This secular value reproduces the evolution from equation (36) very well, as shown by the dashed lines in Fig. 13.

Using this secular expression for $Z(v_{\rm h})$, taking $v_\star = 400$ km s^{-1}, and $y = 0.04$, $Z_\odot = 0.0127$ for the total metal yield and solar metallicity as done in the stellar evolution models collected from

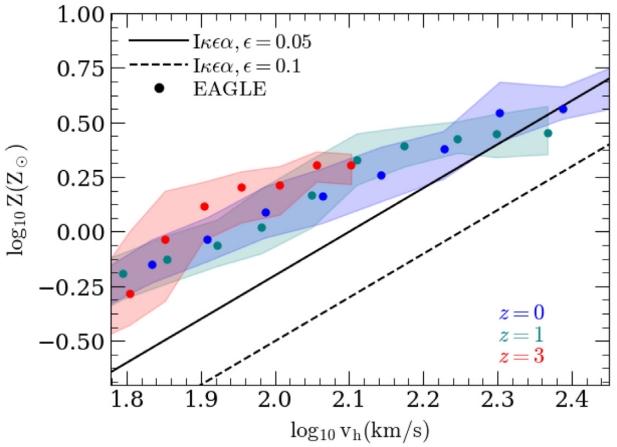

Figure 12. Metallicity, Z, of the star-forming gas as a function of the halo's circular velocity, $v_{\rm h}$, at various redshifts. The large solid dots are the median relation from EAGLE (simulation FbconstnoAGN), with the shaded area encompassing the 25–75th percentile for redshifts $z = 0$ (blue), 1 (green), and 3 (red). Only haloes with at least 10^3 gas particles are shown. The black lines correspond to the $I\kappa\epsilon\alpha$ model, from equation (38), with $\epsilon = 0.05$ and 0.1 shown as a *solid* and *dashed line*, respectively; the redshift dependence of these lines is negligible, and the results depend very little on the assumed initial metallicity. The dependence of Z on $v_{\rm h}$ is slightly shallower in EAGLE compared to $I\kappa\epsilon\alpha$. The Z–$v_{\rm h}$ relation is almost independent of redshift in both the model and EAGLE.

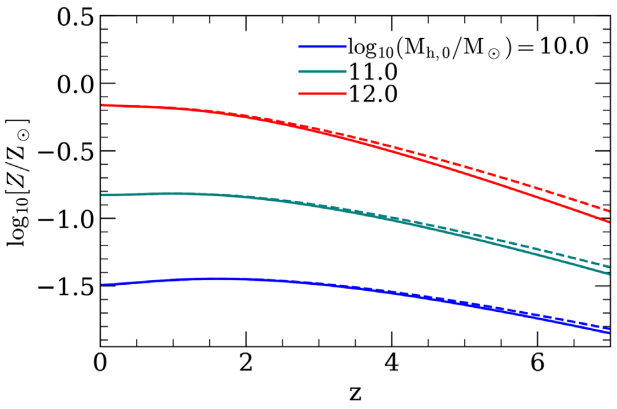

Figure 13. Metallicity, Z, in solar units, as a function of redshift, z, for haloes with different mass; (*blue*, *green*, *and red* correspond to $z = 0$ halo masses of $\log_{10} M_{\rm h,0}/{\rm M}_\odot = 10$, 11, and 12, respectively). The result from integrating equation (36) numerically is shown as *solid lines*, and the approximation $Z = \kappa y {v_{\rm h}}^2/v_\star^2$ is shown as *dashed lines*. Results are shown taking $v_\star = 400$ km s^{-1}, $y = 0.04$, and $Z_\odot = 0.0127$.

the literature by Wiersma et al. (2009), we obtain

$$\frac{Z}{0.68\times {\rm Z}_\odot} = \left(\frac{M_{\rm h,0}}{10^{12}\,{\rm M}_\odot}\right)^{2/3} (m_{\rm h}\mathcal{H})^{2/3} = \left(\frac{\dot{M}_\star}{1.2\,{\rm M}_\odot\,{\rm yr}^{-1}}\right)^{2/5} \frac{(m_{\rm h}\mathcal{H})^{2/3}}{\Psi_\star^{2/5}} = \left(\frac{M_\star}{1.7\times 10^{10}\,{\rm M}_\odot}\right)^{2/5} \frac{(m_{\rm h}\mathcal{H})^{2/3}}{m_\star^{2/5}}. \quad (38)$$

The reference values of $\dot{M}_\star$ and $M_\star$ for the star formation rate and stellar mass are taken from equations (16) and (18), respectively. The normalization of this relation, $0.68\,{\rm Z}_\odot$ for $M_{\rm h,0} = 10^{12}\,{\rm M}_\odot$, depends on $I\kappa\epsilon\alpha$ parameters $\propto (\kappa\alpha/(\epsilon\eta))^{3/5}$. The observed normalization is uncertain but at face value higher than what we find by a factor of 2 (e.g. Tremonti et al. 2004).

The dependence of Z on $v_{\rm h}$ implies that $I\kappa\epsilon\alpha$ galaxies fall on a mass–metallicity relation, as well as on a star formation rate–metallicity relation. Similarly to the stellar mass–halo mass relation, we can compute how Z depends on $M_\star$ at a given redshift,

$$\frac{{\rm d}\ln Z}{{\rm d}\ln M_\star}|_{z=\rm const} = \frac{{\rm d}\ln Z}{{\rm d}\ln \dot{M}_\star}|_{z=\rm const} = \frac{2}{5}, \quad (39)$$

independent of redshift, with the value of the exponent resulting from the ${v_{\rm h}}^2 \propto M_\star^{2/5}$ dependence of equation (18). As a galaxy grows in mass, its metallicity increases as

$$\frac{{\rm d}\ln Z}{{\rm d}\ln M_\star}|_{M_{\rm h,0}=\rm const} = \frac{2}{3}\frac{{\rm d}\ln(m_{\rm h}\mathcal{H})/{\rm d}z}{{\rm d}\ln m_\star/{\rm d}z}. \quad (40)$$

The evolution of Z at a *given* stellar mass or star formation rate is $\propto (m_{\rm h}\mathcal{H})^{2/3}$ according to equation (38). With increasing z, $m_{\rm h}(z)$ decreases whereas $\mathcal{H}(z)$ increases, resulting in little evolution in the Z–$M_\star$ relation. At a given value of $M_\star$, Z decreases with increasing z by factors of 0.9 and 0.76 compared to its $z = 0$ value for $z = 2$ and 3, respectively. The observed evolution is somewhat stronger and better reproduced by the EAGLE REFERENCE model in which ϵ varies with the local gas properties (De Rossi et al. 2017).

Why does Z depend on $M_\star$ in $I\kappa\epsilon\alpha$? The $I\kappa\epsilon\alpha$ metallicity of a galaxy is $Z \approx y\dot{M}_\star/(\omega_{\rm b}\dot{M}_{\rm h})$, the ratio of the rate at which stars metal enrich the ISM over the rate at which these metals are being diluted by accreting (primordial) gas. The reason this ratio depends on $M_\star$ is that the star formation efficiency depends on $v_{\rm h}$: $\dot{M}_\star/(\omega_{\rm b}\dot{M}_{\rm h}) \propto {v_{\rm h}}^2 \propto M_\star^{2/5}$, given that $M_\star \propto {v_{\rm h}}^5$. In $I\kappa\epsilon\alpha$, *the origin of the mass–metallicity relation is the dependence of the star formation efficiency on the halo's virial velocity. The $M_\star$–Z relation evolves because the $M_\star$–v_h relation evolves.* The first part of this claim agrees with Davé et al. (2012), but the second part does not: In their model, evolution is caused by the increase in metallicity of accreting gas. Note that, as long as the galaxy self-regulates[8] its gas metallicity is set by the instantaneous star formation rate rather than a consequence of the build-up of metals that fail to escape from the potential well of its host halo. In other words, the reason that Z depends on $v_{\rm h}$ is because $\dot{M}_\star/\dot{M}_{\rm h}$ depends on $v_{\rm h}$, rather than that it is 'easier for metals to escape from haloes with low $v_{\rm h}$', as is often claimed. Indeed, we have assumed that $Z_{\rm w} = Z$ so that an outflow by itself does not affect Z *at all*. Instead, low-$v_{\rm h}$ haloes have galaxies with low Z because they are inefficient at forming stars.

3.4 When stellar feedback fails

The basic $I\kappa\epsilon\alpha$ relation of equation (15) between the halo accretion rate and the star formation rate results in $\dot{M}_\star \propto v_{\rm h,0}^5$, where $v_{\rm h,0}$ is the virial velocity of the halo at redshift $z = 0$, so that haloes with a large virial velocity form stars at a greater rate. For low values of $v_{\rm h,0}$, only a very small fraction of the accreted baryons are converted into stars with the majority of the accreted gas expelled in an outflow, as discussed in Section 3.1. The rate of gas accretion increases $\propto v_{\rm h,0}^3$ but the star formation rate increases $\propto v_{\rm h,0}^5$. Since obviously the star formation rate cannot be higher than when *all* accreted gas is converted to stars, $\dot{M}_\star \le \omega_{\rm b}\dot{M}_{\rm h}$, it eventually becomes impossible to satisfy equation (15) when $v_{\rm h}$ is larger than the critical value that

[8]Clearly, this would not be true in case of a recent merger that might increase $\dot{M}_\star$ *and* dilute Z by gas accretion.

results from inserting $\dot{M}_\star = \omega_\mathrm{b}\dot{M}_\mathrm{h}$ in equation (15),

$$v_{\mathrm{h,max}} = \frac{v_\star}{\kappa^{1/2}} = 310\frac{v_\star/400\,\mathrm{km\,s^{-1}}}{(\kappa/(5/3))^{1/2}}\,\mathrm{km\,s^{-1}}. \quad (41)$$

Equation 31 gives a slightly weaker limit when requiring that the mass-loading factor $\beta \geq 0$ so that any outflow decreases the baryon fraction of the halo rather than spuriously increasing it.

As a halo grows and v_h increases, β starts to drop rapidly to values below 1, as seen in Fig. 10. At $z \leq 2$, $\beta \to 0$ for $v_\mathrm{h} \to v_{\mathrm{h,max}}$ but β already plunges to values $\beta \leq 1$ as v_h approaches a somewhat smaller critical velocity. At higher redshifts, this critical halo virial velocity decreases, basically because it is no longer a good approximation to neglect $\dot{M}_\mathrm{gas}$.

What is the consequence of this failure of self-regulation for haloes with too high v_h? The $I\kappa\epsilon\alpha$ GSMF discussed in Section 2.6 is a power law that tracks the power-law shape of the halo-mass function. In contrast, the *observed* GSMF has an exponential cut-off at stellar masses above a characteristic stellar mass. It is thought that feedback from accreting black holes (AGNs) suppresses star formation in such massive galaxies and this is the cause of the observed break in the GSMF (e.g. Bower et al. 2006; Croton et al. 2006).

This motivates us to associate the critical velocity above which stars cannot self-regulate galaxy formation with those haloes in which AGNs regulate galaxy formation instead. Using the subscript 'agn' as a mnemonic, we see from Fig. 10 that the onset of AGN activity takes place at a nearly redshift-independent value of v_h of the order of

$$v_{\mathrm{h,agn}} \approx 180\,\mathrm{km\,s^{-1}}, \quad (42)$$

for which the corresponding virial temperature is[9]

$$T_{\mathrm{h,agn}} = \frac{\mu m_\mathrm{p} v_{\mathrm{h,agn}}^2}{5k_\mathrm{B}} \approx 10^{5.7}\,\frac{\mu}{0.62}\left(\frac{v_{\mathrm{h,agn}}}{180\,\mathrm{km\,s^{-1}}}\right)^2\,\mathrm{K}. \quad (43)$$

In the model described by Bower et al. (2017), seed black holes start to grow exponentially in mass when the outflow that is powered by feedback from star formation ceases to be buoyant in the hot corona that fills the dark matter halo. This causes a build-up of gas that fuels the growth of the black hole. The episode of exponential growth ends when the black hole is sufficiently massive that its feedback regulates the forming galaxy. In practice, this results in a significant decrease in $\dot{M}_\star/M_\star$. This model describes well the behaviour of galaxies in the EAGLE simulation, with the transition between star formation and AGN feedback-regulated galaxies occurring in haloes with a virial temperature nearly identical to that of equation (43) (McAlpine et al. 2018).

At first sight, it seems that the reasoning that led to equation (43), 'stellar feedback fails because $v_\star^2$, a measure of the thermal energy of feedback-heated gas, is too low compared to $\kappa {v_\mathrm{h}}^2$' is very different from that of Bower et al. (2017), 'stellar feedback fails because outflows are no longer buoyant in the hot corona'. However, the build-up of the hot halo is itself depending on the efficiency of stellar feedback (Correa et al. 2018). Put in terms of $I\kappa\epsilon\alpha$: the higher ϵ, the higher the value of v_h above which a hot corona develops (see in particular fig. 14 in Correa et al. 2018). Within the current interpretation, the failure of stellar feedback is not due to the formation of a hot corona, but rather the formation of a hot halo is facilitated by failing stellar feedback.

[9] m_p is the proton mass, k_B is Boltzmann's constant, and μ the mean molecular weight.

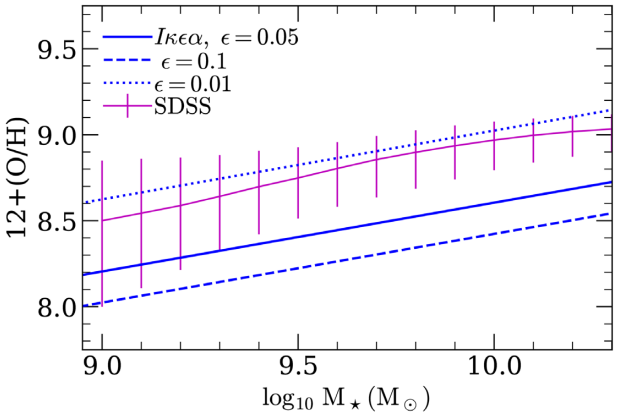

Figure 14. Metallicity 12 + (O/H) as a function of the stellar mass, $M_\star$, from $I\kappa\epsilon\alpha$ for feedback efficiency $\epsilon = 0.01$ (*dotted blue*), 0.05 (*solid blue*), and 0.1 (*dashed blue*). The $I\kappa\epsilon\alpha$ results (solid lines) have been obtained by integrating equation (36), for a yield, $y = 0.04$ and then converted to the units of 12 + (O/H) assuming that a metallicity of $Z = Z_\odot = 0.0127$ corresponds to 12 + (O/H)=8.7. For a comparison, the observed trend at $z = 0$ for SDSS galaxies (Mannucci et al. 2010) is also shown as a thin magenta line with vertical bars for the scatter. $I\kappa\epsilon\alpha$ reproduces the slope of the Z–$M_\star$ relation very well.

The results from the previous sections allow us to compute other properties of the halo and the galaxy when $v_\mathrm{h} = v_{\mathrm{h,agn}}$, the onset of AGN activity. The halo mass, stellar mass, and star formation rate in a halo with $v_\mathrm{h} = v_{\mathrm{h,agn}}$ at $z = 0$ are

$$\begin{aligned} M_{\mathrm{h,agn}}(z=0) &= 2\times10^{12}\,\mathrm{M_\odot}\,\frac{(v_{\mathrm{h,agn}}/180\,\mathrm{km\,s^{-1}})^3}{\alpha/1} \\ M_{\star,\mathrm{agn}}(z=0) &= 5.3\times10^{10}\,\mathrm{M_\odot}\left(\frac{v_{\mathrm{h,agn}}}{180\,\mathrm{km\,s^{-1}}}\right)^5 \\ \dot{M}_{\star,\mathrm{agn}}(z=0) &= 3.8\,\mathrm{M_\odot\,yr^{-1}}\left(\frac{v_{\mathrm{h,agn}}}{180\,\mathrm{km\,s^{-1}}}\right)^5, \end{aligned} \quad (44)$$

and the corresponding values at redshift z are

$$\begin{aligned} M_{\mathrm{h,agn}}(z) &= \frac{M_{\mathrm{h,agn}}(z=0)}{\mathcal{H}(z)} \\ M_{\star,\mathrm{agn}}(z) &= M_{\star,\mathrm{agn}}(z=0)\,\frac{m_\star(z)}{(m_\mathrm{h}(z)\mathcal{H}(z))^{5/3}} \\ \dot{M}_{\star,\mathrm{agn}}(z) &= \dot{M}_{\star,\mathrm{agn}}(z=0)\,\frac{\Psi_\star(z)}{(m_\mathrm{h}(z)\mathcal{H}(z))^{5/3}}. \end{aligned} \quad (45)$$

We do not expect the $I\kappa\epsilon\alpha$ GSMF to be correct for haloes with $v_\mathrm{h} \geq v_{\mathrm{h,agn}}$. We therefore plot the GSMF discussed in Section 2.6 up to haloes of mass $M_{\star,\,\mathrm{agn}}(z)$, and compare to the EAGLE GSMF (simulation FbConst, in which the stellar feedback efficiency is a constant and which *does* include feedback from an AGN) in Fig. 15. The $I\kappa\epsilon\alpha$ model reproduces the power-law shape of the EAGLE mass function up to $M_{\mathrm{h,agn}}(z)$ well, getting the evolution of the normalization approximately correct as well. The value of $M_{\star,\,\mathrm{agn}}(z)$ is close to where EAGLE predicts a rapid decrease in the number density of galaxies, which is due to the action of AGN feedback in the simulation. The number density of galaxies at the knee decreases with increasing z. The previous equations elucidate the reason for this in $I\kappa\epsilon\alpha$. Consider two redshifts z_1 and z_2, with $z_1 < z_2$, say. Haloes with $v_\mathrm{h} = v_{\mathrm{h,agn}}$ at a redshift z_2 will be more massive at $z = 0$ than those that have $v_\mathrm{h} = v_{\mathrm{h,agn}}$ at a redshift z_1, by the factor $\mathcal{H}(z_2)/\mathcal{H}(z_1)$, which is $\approx((1+z_2)/(1+z_1))^{3/2}$ for $z_1 \geq 1$. The corresponding ratio of number densities then follows from the

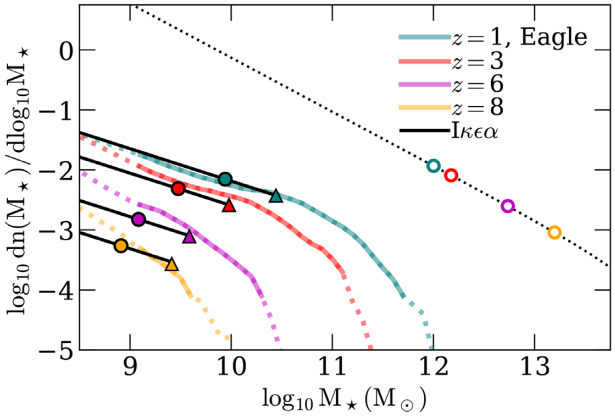

Figure 15. The evolution of the GSMF. The *coloured curves* show the EAGLE GSMF (simulation FbConst, in which the feedback efficiency is constant and which includes AGN feedback), with results at $z = 1$, 3, 6, and 8 shown in *green*, *red*, *purple*, and *yellow*, respectively. At high mass, the curves are drawn as *dashed lines* if there are fewer than 5 galaxy dex in $\log_{10}M_\star$, at low mass when there are fewer than 100 stellar particles per galaxy. The *black full lines* are the corresponding *I*$\kappa\epsilon\alpha$ results from Section 2.6, with a *triangle* corresponding to galaxies of mass $M_{\star,\,\mathrm{agn}}$ (equation 45) above which feedback from an AGN is expected to set in, and a *filled circle* at half this mass. The *black dotted line* is the halo-mass function (equation 22). The *coloured open circles* indicate the abundance of haloes with mass $M_{\mathrm{h,agn(z)}}/2$, computed from equation (45). The *I*$\kappa\epsilon\alpha$ model predicts the shape and evolution of the normalization of the EAGLE GSMF well. The predicted location of the knee in the GSMF is also reasonable. We used $a = \bar{a}$ and $b = \bar{b}$ for the accretion history of haloes (equation 7).

slope of the PS halo-mass function, $(\mathcal{H}(z_2)/\mathcal{H}(z_1))^{\alpha_\mathrm{h}}$. For example, the comoving number density at $z = 6$ is lower than at $z = 1$ by a factor of 4.8.

3.5 Reality check

Up to now, we have compared *I*$\kappa\epsilon\alpha$ to an EAGLE simulation in which the feedback parameters are kept constant (simulation FbConst). That simulation does not reproduce the observed properties as well as the EAGLE reference simulation. So, how well does *I*$\kappa\epsilon\alpha$ describe the observations?

For a fiducial value of $v_\star = 400$ km s^{-1}, *I*$\kappa\epsilon\alpha$ predicts that a $z = 0$ galaxy with a stellar mass $M_\star = 5 \times 10^{10}\,\mathrm{M}_\odot$ has a star formation rate of $\dot{M}_\star = 3.5\,\mathrm{M}_\odot\,\mathrm{yr}^{-1}$ and is hosted in a dark matter halo of mass $M_\mathrm{h} = 1.9 \times 10^{12}\,\mathrm{M}_\odot$. For the Milky Way, the inferred values are $M_\star = (5 \pm 1) \times 10^{10}\,\mathrm{M}_\odot$, $\dot{M}_\star = (1.65 \pm 0.19)\,\mathrm{M}_\odot\,\mathrm{yr}^{-1}$, and $M_\mathrm{h} = (1.1 \pm 0.3) \times 10^{12}\,\mathrm{M}_\odot$ (Bland-Hawthorn & Gerhard 2016), respectively. However, the scatter in $M_\star$ and $\dot{M}_\star$ for a halo with given M_h is substantial, and the *I*$\kappa\epsilon\alpha$ value for $M_\star$ is consistent with the abundance matching analysis by Guo et al. (2010), and the star formation rate of $\dot{M}_\star = 3.5\,\mathrm{M}_\odot\,\mathrm{yr}^{-1}$ falls well within the blue cloud for a galaxy with that $M_\star$ in the MPA-JHU DR7[10] catalogue. This reasonable level of agreement is of course not surprising: We chose *I*$\kappa\epsilon\alpha$'s feedback efficiency parameter ϵ that sets $v_\star$ by comparing to these data sets.

The *I*$\kappa\epsilon\alpha$ sSFR is $\dot{M}_\star/M_\star \approx 0.07\,\mathrm{Gyr}^{-1}$ at $z = 0$, *independent of* ϵ, as compared to an observed value of $0.1\,\mathrm{Gyr}^{-1}$ at $M_\star = 10^{10}\,\mathrm{M}_\odot$ (see the discussion of the data compilation by Behroozi et al. 2018). The observed sSFR increases to a value of $1\,\mathrm{Gyr}^{-1}$ ($2\,\mathrm{Gyr}^{-1}$) by redshift $z = 1$ ($z = 2$, Behroozi et al. 2018), as compared to the *I*$\kappa\epsilon\alpha$ values of 0.3 (1). The *I*$\kappa\epsilon\alpha$ values are actually very close to those in EAGLE (simulation FbConstNoAGN). The faster observed evolution might signal that ϵ does evolve.

The $M_\star \propto M_\mathrm{h}^{5/3}$ dependence of stellar mass on halo mass according to equation (18) results in a redshift-independent low-mass slope of the GSMF of $\mathrm{d}n/\mathrm{d}\log(M_\star) \propto M_\star^{\approx -0.54}$. The faint-end slope of the Schechter luminosity function (Schechter 1976),

$$\frac{\mathrm{d}n(L)}{\mathrm{d}\log L} \propto L^{-\alpha_\mathrm{g}}\,\exp(-L/L_\star), \tag{46}$$

is $\alpha_\mathrm{g} \approx 0.48$ at redshift $z = 0$ in the GAMA 'z' band (Loveday et al. 2012), a long enough wavelength so that stellar mass is approximately proportional to z-band luminosity. The level of agreement between the two slopes, 0.54 versus 0.48, is encouraging, but not surprising given that *I*$\kappa\epsilon\alpha$ reproduces the EAGLE GSMF at the low-mass end well (Fig. 15). Observationally, there is no convincing evolution of this slope out to $z \sim 3$ in the K band (Mortlock et al. 2017), also consistent with the *I*$\kappa\epsilon\alpha$ prediction of no evolution.

The observed evolution in the location of the knee of the Schechter luminosity function is claimed to be consistent with little or no evolution in the value of the *stellar mass* at which the transition occurs (e.g. Song et al. 2016) but an alternative interpretation is that the transition occurs at a nearly constant star formation rate. Indeed, according to Parsa et al. (2016), the absolute 1500 Å magnitude of galaxies at the knee of the Schechter luminosity function occurs at $M_{1500,\,\mathrm{c}} = -19.6$, -20.3, -20.6, and -20.68 for redshifts $z = 1$, 2, 3, and 4, respectively. If we make the reasonable assumption that UV luminosity is proportional to star formation rate, then the star formation rate $\dot{M}_\star$ of those galaxies increases compared to the value at $z = 1$ by factors $\dot{M}_\star(z)/\dot{M}_\star(z = 1) = 1.9$, 2.5, 2.8, and 2.9 at $z = 2$, 3, 4, and 5. The prediction from *I*$\kappa\epsilon\alpha$ follows from equation (45), $\dot{M}_{\star,\mathrm{agn}}(z)/\dot{M}_{\star,\mathrm{agn}}(z = 1) = 1.6$, 2.2, 2.8, and 3.4, respectively, impressively close to the observations.

We conclude from this brief comparison to data that *I*$\kappa\epsilon\alpha$ reproduces observations of the observed galaxy population and its evolution rather well, although there are some differences too.

3.6 Incorporating AGN feedback

An important limitation of the model as described so far is the absence of AGN feedback. Following the arguments that led us to stellar-feedback self-regulation, an obvious way to include AGNs in the model is by modifying equation (15) to

$$\frac{1}{2}\dot{M}_\star\, v_\star^2 + \frac{1}{2}\dot{M}_\mathrm{BH}\, v_\mathrm{agn}^2 = \frac{\kappa}{2}\omega_\mathrm{b}\,\dot{M}_\mathrm{h} {v_\mathrm{h}}^2$$
$$v_\mathrm{agn}^2 = \frac{2\epsilon_\mathrm{r}\epsilon_\mathrm{f}}{1-\epsilon_\mathrm{r}}c^2, \tag{47}$$

with the understanding that AGN feedback sets in when[11] $v_\mathrm{h} \gtrapprox v_\mathrm{h,agn}$. Here, $\epsilon_\mathrm{r} \approx 0.1$ is the radiative efficiency of the AGN and $\epsilon_\mathrm{f} \approx 0.15$ the fraction of radiated energy that couples to the gas (see the discussion in Schaye et al. 2015, their section 4.6). As in the case of feedback from star formation discussed in Section 2.4.1, AGN feedback will be self-regulating provided that the black hole accretion rate *increases* with the pressure in the ISM.

[10] https://wwwmpa.mpa-garching.mpg.de/SDSS/DR7/

[11] v_agn, which characterizes the energy input by the AGN per unit of mass accreted on to the BH, is not to be confused with $v_\mathrm{h,agn}$ – the virial velocity of the halo above which stellar feedback fails.

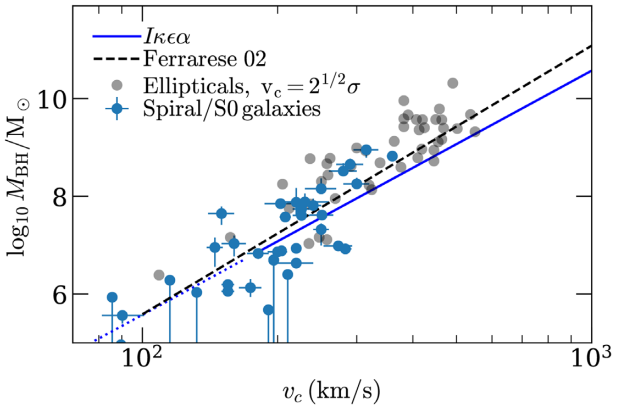

Figure 16. The dependence of black hole mass, M_{BH}, on the circular speed of the host halo, v_c. The *blue line* is the trend from $I\kappa\epsilon\alpha$, equation (48), with v_h scaled to v_c following Ferrarese (2002); the trend originally proposed by Ferrarese (2002) is shown as a *dashed black line*. Data points are taken from the compilation by Kormendy & Ho (2013); the *blue circles* with error bars are spiral and S0 galaxies and the *grey circles* are elliptical galaxies.

We can examine what to expect for the black hole mass of a halo with $v_h \gg v_{h,agn}$ by integrating equation (47) for $v_\star = 0$,

$$M_{BH} = \frac{3}{5}\frac{\kappa\omega_b}{\alpha^{3/2}}\frac{v_h^5}{10H(z)Gv_{agn}^2} = 1.2\times10^7\frac{(v_h/200\ \mathrm{km\ s^{-1}})^5}{(\epsilon_r\epsilon_f/(1-\epsilon_r))/(0.1\times0.07)}\mathrm{M}_\odot, \quad (48)$$

where the second line is at redshift $z = 0$; this scaling is plotted as a blue line in Fig. 16. How does this compare to observations? Ferrarese (2002) claim that black hole mass scales with the circular speed as $M_{BH} \propto v_c^{5.5}$. This scaling is shown as a black dashed line and is close to equation (48). Kormendy & Ho (2013) argue that, because the scatter in the M_{BH}–v_c relation is large at low v_c, the *Magorrian relation* (Magorrian et al. 1998) between black hole mass and bulge mass is more fundamental. We would argue instead that low-mass black holes are not in a self-regulating regime.

The observed relation between black hole mass and (3D)[12] stellar velocity dispersion $\sigma_\star$ is $M_{BH} = 1.1\times10^7\,(\sigma_\star/200\ \mathrm{km\ s^{-1}})^{5.12}\ \mathrm{M}_\odot$ (McConnell et al. 2011). Provided $v_h \sim \sigma_\star$, the observed dependence on velocity is close to our prediction while the normalization requires reasonable values for ϵ_r and ϵ_f. The scaling of the M_{BH}–$\sigma_\star$ relation in the model by Silk & Rees (1998) is identical to ours basically because both are based on energy arguments; however, our normalization is significantly more realistic, as shown in Fig. 16. The model by King (2003) is based on momentum arguments; their scaling, $M_{BH} \propto \sigma_\star^4$, is shallower than observed. Booth & Schaye (2010) obtain an $M_{BH} \propto M_h^{1.55}$ scaling by arguing that the net total energy injected by an AGN is of the order of the binding energy of a halo. This is somewhat similar to our reasoning, except that we argue that it is the *rate* of energy injection by the AGN that tracks the *rate* of energy accretion by the halo due to self-regulation. The secular growth rate of a black hole – and hence the time-averaged luminosity of the AGN – therefore depends on the cosmological accretion rate on to its host halo and therefore on redshift, and not just on halo properties.

[12]We have assumed that $\sigma_\star^2 = 3\sigma^2$, where σ is the line-of-sight stellar velocity dispersion.

4 DISCUSSION

4.1 Comparison to previous work

The paper by Bouché et al. (2010) sparked interest in trying to understand the basic physics underlying self-regulation of galaxies. That paper, and several that followed, contains equations that resemble those of Section 3, but the underlying assumptions are sometimes strikingly different, as we discuss here. The starting point of Bouché et al. (2010) is their realization that the dependence of $\dot{M}_\star$ on stellar mass and redshift resembles that of the cosmological accretion rate, suggesting that the gas accretion rate $\dot{M}_{gas,acc} \propto \dot{M}_h$. The proportionality constant is argued to be less than ω_b, the cosmological gas-to-total matter density, because only cold accreted gas is assumed to be eligible for star formation. The resulting star formation rate is then determined by the efficiency with which gas is converted into stars, that is, by the star formation law.

This reasoning results in $\dot{M}_\star \propto \omega_b\dot{M}_h$, as in our equation (16), with the important distinction that the efficiency of galaxy formation,

$$\epsilon_g \equiv \frac{\dot{M}_\star}{\omega_b\dot{M}_h}, \quad (49)$$

is set by the efficiency of star formation,

$$\epsilon_\star \equiv \frac{\dot{M}_\star}{M_{gas}/\tau_d}, \quad (50)$$

where τ_d is a characteristic time that still needs to be determined. The onus of getting the observed $M_\star/M_h$ relation is now wholly on the star formation law (equation 50). The solution advocated by Bouché et al. (2010) is to assume that haloes do not form any stars as long as their halo mass is below some minimum value, $M_{h,\,min} \approx 10^{10}$–$10^{11}\ \mathrm{M}_\odot$, which conspires to result in ϵ_g increasing with M_h. They stress repeatedly that their results are completely independent of the efficiency of feedback.

Lilly et al. (2013) build on this work, and in their 'gas-regulator' framework, $\dot{M}_\star$ is regulated by the gas reservoir of the galaxy, M_{gas} in our notation. Rather than assuming a minimum halo mass $M_{h,\,min}$ below which no stars form, the model introduces two main fitting parameters, which in our notation are the product $\epsilon_\star\,\tau_d$ (their variable ϵ) and β (their variable λ). In the follow-up paper by Birrer et al. (2014), they show how the evolution of galaxies over cosmic time can be modelled well once ϵ and λ are parametrized as functions of $M_\star$. Note that these cannot be independent of $M_\star$, since otherwise the ratio $M_\star/M_h$ is constant as well, since a constant fraction of the accreted gas is converted into stars.

The 'minimum bath-tub' model described by Dekel & Mandelker (2014) has very similar ingredients, in that $\dot{M}_\star$ is also regulated by M_{gas} through the star formation law. These authors stress that many properties of galaxies follow from this model if it is assumed that the system is in a quasi-steady state, $\dot{M}_{gas} = 0$.

These models 'self-regulate' in the sense that the star formation rate is determined by the gas mass by mass conservation, in our notation $\dot{M}_{gas} = \omega_b\dot{M}_h - (1-\mathcal{R}+\beta)\dot{M}_\star$ (equation 30), so that too much star formation depletes the gas reservoir, which ultimately decreases $\dot{M}_\star$. Conversely, too little star formation leads to a build-up of M_{gas}, and through the star formation law, this increases $\dot{M}_\star$. A very nice feature of these models, in addition to predicting correctly the rapid increase in $\dot{M}_\star/M_\star$ with redshift because the gas accretion rate $\propto \dot{M}_h$, is that they correctly predict secondary parameter dependences, for example the fact that galaxies that lie

above the main sequence are more gas rich and more metal poor; see also Dayal et al. (2013).

What all these models have in common is that the star formation rate is set by the gas reservoir through the star formation law. The origin of that law is not discussed in detail, but presumably it results from a balance between cooling and heating from star formation, as originally envisioned by White & Frenk (1991). In these models, feedback from star formation is only important in setting the star formation law, basically parametrized by $\epsilon_\star$. Combined with a model for the build-up of dark matter haloes, or using dark matter-only simulations that follow the growth of haloes, these 'self-regulation' models are very successful in building realistic looking mock universes (see e.g. Moster, Naab & White 2018; Tacchella et al. 2018).

In our opinion, there are two major weaknesses to this basic model: (*i*) to be predictive, the model needs to be able to predict how the efficiency of star formation, $\epsilon_\star$, and the mass-loading factor, β, depend on halo (or stellar mass), which is a formidable task. More worryingly, (*ii*) there is evidence that one of the main assumptions – that the star formation rate depends on the gas mass through the star formation law – is not quite correct.

At first sight, it seems impossible that the rate of star formation in a galaxy is not dependent on the star formation law, and in fact it would be if the galaxy were isolated. However, a galaxy in a cosmological setting can gain mass through accretion and lose it through winds, and therefore the amount of gas in the reservoir is not some constant, rather $M_{\rm gas}$ too is set by the physics of galaxy formation. Demanding that $\dot{M}_\star$ depends on $M_{\rm gas}$ through a star formation law, and vice versa, results in a 'chicken and egg' problem.

Numerical simulations can be very helpful in distinguishing cause from effect. The OWLS simulations described by Schaye et al. (2010) are cosmological hydrodynamical simulations performed with GADGET (Springel 2005), but the parameters of subgrid models are varied over a very wide range and not calibrated to observations as in EAGLE. In particular, the OWLS simulation suite includes parameter variations in which the efficiency of feedback from stars (*i.e.* the value of $v_\star$ in our notation) and the star formation law (the values of A and n in equation A2) are varied separately. By plotting $M_{\rm gas}$ and $\dot{M}_\star$ versus a variable that does not depend on either $v_\star$ or the star formation law, such as halo mass, $M_{\rm h}$, it becomes possible to test the very core assumption of the gas-regulator or bath-tub models.

Haas et al. (2013a) compare models with the same star formation law (same value of A and n) but different values of the feedback efficiency. Compare, in particular, their models REF and WML4: These have identical numerical parameters, except that the value of $v_\star^2$ in simulation WML4 is twice that of REF. Maybe not surprisingly, $\dot{M}_\star/M_{\rm h}$ in the simulation with the stronger feedback is about half as large as in REF (their fig. 4). Because the star formation law in these simulations is the same, this also implies that $M_{\rm gas}/M_{\rm h}$ is also approximately half in WLM4 compared to REF, as is also born out by the same figure.

However, now compare models REF and SFAMPLx3 in Haas et al. (2013b): These have identical feedback parameters, but the value of A (from equation A2) in simulation SFAMPLx3 is three times that in simulation REF. Fig. 5 in Haas et al. (2013b) shows that nevertheless the ratio $\dot{M}_\star/M_{\rm h}$ is nearly identical in the two simulations: The star formation rate in a halo of given mass is not, or only very weakly dependent, on A: a direct violation of the main assumption in the 'gas-regulator' models. Given that the star formation rates are the same in these models, but the star formation law differs, this must imply that the gas reservoir in SFAMPLx3 is less than that in REF at a given value of $M_{\rm h}$: The same Fig. 5 shows that indeed $M_{\rm gas}/M_{\rm h}$ is about a factor of 3 lower in model SFAMPLx3 compared to REF. As stressed by Haas et al. (2013b) and confirming what was found by Schaye et al. (2010), stellar feedback regulates the star formation rate by determining the amount of (star forming) gas. In this interpretation, *$\dot{M}_\star$ regulates $M_{\rm gas}$ through stellar feedback, rather than $M_{\rm gas}$ setting $\dot{M}_\star$ through a star formation law*.

The model presented by Davé et al. (2012) incorporates self-regulation through feedback, as envisioned here. Because they limit their analysis to equilibrium states defined by $\dot{M}_{\rm gas} = 0$, their results are actually very similar to the various incarnations of the bath-tub models.

In our interpretation, self-regulation follows from energy conservation, equation (15), and in particular the fact that $\dot{E}_{\rm g} = 0$ is a secularly stable equilibrium (provided that $\dot{\rho}_\star$ increases with pressure of the star-forming gas). Therefore, accretion sets the star formation rate, once the net energy input generated by forming stars is known. This sets the 'efficiency of galaxy formation' (the ratio of the star formation rate over the cosmological baryon accretion rate on to a halo) to be

$$\frac{\dot{M}_\star}{\omega_{\rm b}\dot{M}_{\rm h}} = \kappa\frac{v_{\rm h}^2}{v_\star^2}\,, \tag{51}$$

which does not depend on the star formation law but on the properties of the halo (through $v_{\rm h}$) and the efficiency of feedback (through $v_\star$). This is in contrast to equation (50). The star formation law then determines the gas reservoir in the $I\kappa\epsilon\alpha$ model, with any excess accreted gas expelled in a wind.

The relation between stellar mass and halo mass (equation 18) can be cast in the form

$$\log_{10}\left(\frac{M_\star}{10^{12}\,{\rm M}_\odot}\right) = \frac{5}{3}\log_{10}\left(\frac{M_{\rm h}}{10^{12}\,{\rm M}_\odot}\right) + \log_{10}\mathcal{N}(z)$$
$$\log_{10}\mathcal{N}(z) = \log_{10}\left(\frac{1.7\times10^{10}\,{\rm M}_\odot}{10^{12}\,{\rm M}_\odot}\,\frac{1-\mathcal{R}}{0.55}\,\frac{m_\star(z)}{m_{\rm h}(z)^{5/3}}\right), \tag{52}$$

which has the form of equation (1) in the paper by Salcido, Bower & Theuns (2019), with their $\epsilon(M_{\rm h}, z) = 5/3$. These author show that a halo mass–stellar mass of this form can be integrated to give analytical relations for the GSMF and the evolution of the cosmic star formation rate density.

4.2 Limitations of the model

A forming galaxy can fail to be able to attain its equilibrium star formation rate given by equation (15) for several reasons. Consider for example what happens if $\dot{M}_{\rm h}$ suddenly decreases – for example, because the galaxy becomes a satellite. Star formation will nevertheless continue in accordance with the star formation law, depleting the gas reservoir. In such galaxies, the star formation rate is set by the gas consumption time-scale, rather than regulated by feedback. A less extreme version of the same phenomenon occurs when $\dot{M}_{\rm h}$ for a particular halo is unusually small compared to the ensemble average. The $I\kappa\epsilon\alpha$ model does not correctly describe this situation and in particular is not applicable to satellite galaxies.

We have neglected the finite lifetimes of massive stars. We think this is unlikely to be a major limitation at lower redshifts when the dynamical time of any galaxy is *much* larger than the lifetimes of massive stars. However, the limitation may affect the onset of star formation in small galaxies at high redshift. When $v_{\rm h}$ is very low,

gas cannot cool and our self-regulation argument will not correctly predict $\dot{M}_\star$. When the halo grows in mass it may pass the threshold where gas can cool on a short time-scale, and star formation may be unable to self-regulate because of the finite lifetimes of massive stars. This may lead to a starburst that $I\kappa\epsilon\alpha$ does not model correctly.

Not unrelated is what happens at high values of v_h at low redshift. The $I\kappa\epsilon\alpha$ model predicts that feedback becomes inefficient for $v_\mathrm{h} \approx 180\,\mathrm{km\,s^{-1}}$ following similar reasoning to Bower et al. (2017). We argued, as did Bower et al. (2017), that the resulting increase in gas mass triggers the AGN, which, once the black hole mass has increased sufficiently, will regulate the galaxy. However, by construction this occurs in the same haloes that develop a hot halo of gas, so that it becomes unlikely that the right-hand side of equation (15) describes correctly the rate at which gas enters the galaxy: It may simply add to the hot halo instead [see the discussion in Bouché et al. (2010) on hot versus cold accretion]. We think therefore that it is unlikely that $I\kappa\epsilon\alpha$ models such galaxies accurately. Moreover, galaxy–galaxy mergers contribute significantly to the mass growth of such galaxies, and we have not attempted to include these in the model either.

We also neglected that stars may form from gas lost by previous generations of stars – such recycling may affect the star formation rate of galaxies at late times when their stellar masses are high but the cosmological accretion rate is low (e.g. Oppenheimer et al. 2010; van de Voort 2017). Gas lost from galaxies by winds may re-accrete later – again we have neglected this effect. More in general, we have neglected the possibility that the accretion rate differs from $\omega_\mathrm{b}\dot{M}_\mathrm{h}$.

If equation (15) is indeed applicable, then it might be possible to estimate the scatter around the main sequence of star-forming galaxies from the scatter of $\dot{M}_\mathrm{h}$ around the ensemble average. This would provide a good test of the basic assumption in our model.

5 SUMMARY AND CONCLUSIONS

We have presented a model for star formation in galaxies that is motivated by the origin of the stability of nuclear fusion in main-sequence (MS) stars. The energy generated by nuclear fusion in an MS star equals the rate at which energy is lost through radiation. This equilibrium is secularly stable because if the star loses energy, it heats up, which increases the rate at which fusion occurs. The analogy with a star-forming galaxy is that the rate of energy injection by supernovae (and winds from their massive progenitor stars) equals the rate at which energy is lost due to cosmological accretion. This equilibrium is stable provided the star formation rate increases with the pressure of the star-forming gas.

Equation (15), $(1/2)\dot{M}_\star v_\star^2 = (\kappa/2)\omega_\mathrm{b}\dot{M}_\mathrm{h}\,{v_\mathrm{h}}^2$, encapsulates this energy balance. Here, $v_\star^2$ is a measure of the effective energy injected per unit mass of star formed by feedback, so that the left-hand side is the rate at which feedback increases the galaxy's energy. The right-hand side of the equation is the energy loss term due to cosmological accretion (ω_b is the cosmological baryon-to-total mass fraction), with ${v_\mathrm{h}}^2$ a measure of the depth of the dark halo's potential. In our '$I\kappa\epsilon\alpha$' model, the star formation rate is set by the cosmological accretion rate by energy balance. The predicted dependence of $\dot{M}_\star$ on redshift and virial velocity, v_h, or halo mass, M_h, agrees very well with that measured in the EAGLE cosmological hydrodynamical simulation (Schaye et al. 2015), as shown in Figs 6 and 7, respectively.

The $I\kappa\epsilon\alpha$ model has four parameters (I, κ, ϵ, and α; hence the name), which together shape the star-forming sequence of galaxies. The parameter 'I' stands for the (stellar) **I**nitial mass function (IMF), which sets how much energy is available for feedback from star formation, in particular from the supernovae (SNe) associated with star formation, as well as the recycled fraction $\mathcal{R}$ that relates the time integral of star formation to the stellar mass formed. We have kept the IMF constant in this paper. The dimensionless parameters κ and α quantify the rate of cosmological accretion on to a halo (κ), and the concentration of such haloes (α; see equation 2). We find that $\kappa \approx 5/3$ and $\alpha \approx 1$, and have kept these constant as well.

We think that the main numerical parameter that affects our results is ϵ, which is a measure of the fraction of the energy that is injected by SNe that effectively increases the energy of the star-forming gas, rather than being radiated away. It relates $v_\star^2$ to the energy produced by SNe per unit mass (or more generally to the energy injected in the ISM as a result of recent star formation); see equation (14). If feedback is efficient, ϵ is large, and $\dot{M}_\star$ is small. The EAGLE simulation has a parameter, f_th, that controls what fraction of the available supernova energy is injected into the star-forming gas. This means that $f_\mathrm{th} \approx \epsilon$, provided radiative losses are small. Because feedback *is* efficient[13] in EAGLE, radiative losses in SN-heated gas are mostly small, which explains why the $I\kappa\epsilon\alpha$ model reproduces the EAGLE model with f_th held constant relatively well. However, in the EAGLE REFERENCE model, f_th is allowed to vary as a function of density and metallicity in a way that is calibrated so that the simulation reproduces (some) observations. Therefore, to improve the agreement of $I\kappa\epsilon\alpha$ with data, we would need to understand how radiative losses depend on the ISM of a star-forming galaxy. It seems unlikely that there is a simple way to do so.

A striking feature of the model is that $\dot{M}_\star$ does not depend on the gas mass, M_gas, unlike what is assumed in many self-regulating models (e.g. Bouché et al. 2010; Lilly et al. 2013). We use a star formation law (in our case the Kennicutt–Schmidt law, Kennicutt 1998) to infer M_gas from $\dot{M}_\star$ – rather than the other way around. Doing so allows us to reproduce the M_gas–$\dot{M}_\star$ relation in EAGLE (Fig. 9) as well as the mass–metallicity relation (Fig. 12).

We tried to incorporate feedback from accreting black holes (AGNs) by (*i*) identifying when feedback from star formation fails so that a black hole can grow, and (*ii*) include AGNs in the self-regulation process. Stellar feedback fails in galaxies with deep enough potential wells, so that energy injected by stars cannot compensate for energy lost through accretion even if *all* accreted gas is converted into stars. We showed that this occurs in haloes with virial velocity above a nearly redshift-independent critical value of $\sim$180 km s^{-1}. Demanding that the AGN regulates galaxy formation results in a relation between the black hole mass and the virial velocity of the halo of the form $M_\mathrm{BH} \propto {v_\mathrm{h}}^5$, which closely follows the observed relation.

In the 'Introduction' section, we discussed how gas cooling is thought to play an important role in determining the rate at which a galaxy forms stars, to the extent that it may even be the main property that determines the location of the peak in the redshift evolution of the star formation rate density of the Universe (Hernquist & Springel 2003). Numerical simulations at first sight support this claim directly: A simulation where the contribution from metals is not included when calculating the cooling rate – and hence where the cooling rate is lower – yields lower values of $M_\star/M_\mathrm{h}$ than when metals are included (compare models NOZCOOL and model REF in fig. 3 of Haas et al. 2013a). However, a lower metallicity of star-forming gas reduces cooling losses of injected feedback energy,

[13]Gas heated by SNe has its temperature increased by $\Delta T = 10^7$ K where its cooling rate is minimal and mostly independent of metallicity.

increasing ϵ and hence reducing $\dot{M}_\star$: That sequence of events is also consistent with the findings from Haas et al. (2013a). The main impact of metallicity on the cooling rate of the gas may be on the efficiency of feedback, rather than on the accretion rate. Of course, this argument breaks down in haloes where the virial temperature is so high that most of the gas is and remains hot.

We think that $I\kappa\epsilon\alpha$ provides a simple way of calculating the properties of a galaxy in terms of those of its host halo – and the results thus obtained agree reasonably well with those from much more sophisticated models and importantly also with data. We suggest that a better description of how cooling losses depend on the properties of a galaxy through its history would improve the quality of the theoretical prediction.

ACKNOWLEDGEMENTS

We thank our colleagues (J. Schaye, M. Schaller, R. Crain, and R. Bower) for sharing with us the data from the EAGLE simulation, and we are grateful to L. Heck and J. Helly for providing the computing support. This study was funded by the Science and Technology Facilities Council (grant number ST/F001166/1). The study made use of the DiRAC Data Centric system at Durham University, which is run by the Institute for Computational Cosmology on behalf of the STFC DiRAC HPC Facility (www.dirac.ac.uk); the equipment was funded by BIS National E-Infrastructure capital grant ST/K00042X/1, STFC capital grant ST/H008519/1, and STFC DiRAC, as a part of the National E-Infrastructure. This research was also supported by the Australian Research Council Centre of Excellence for All Sky Astrophysics in 3 Dimensions (ASTRO 3D), through project number CE170100013. The International Centre for Radio Astronomy Research (ICRAR) is a Joint Venture of Curtin University and The University of Western Australia, funded by the Western Australian State government. MS is supported by an ASTRO 3D fellowship at the ICRAR, Curtin University.

REFERENCES

Allen R. J. et al., 2017, ApJ, 834, L11
Behroozi P., Wechsler R., Hearin A., Conroy C., 2018, MNRAS, 488, 3143
Birrer S., Lilly S., Amara A., Paranjape A., Refregier A., 2014, ApJ, 793, 12
Bland-Hawthorn J., Gerhard O., 2016, ARA&A, 54, 529
Bond J. R., Cole S., Efstathiou G., Kaiser N., 1991, ApJ, 379, 440
Booth C. M., Schaye J., 2010, MNRAS, 405, L1
Bouché N. et al., 2010, ApJ, 718, 1001
Bower R. G., Benson A. J., Malbon R., Helly J. C., Frenk C. S., Baugh C. M., Cole S., Lacey C. G., 2006, MNRAS, 370, 645
Bower R. G., Schaye J., Frenk C. S., Theuns T., Schaller M., Crain R. A., McAlpine S., 2017, MNRAS, 465, 32
Chabrier G., 2003, PASP, 115, 763
Correa C. A., Wyithe J. S. B., Schaye J., Duffy A. R., 2015a, MNRAS, 450, 1514
Correa C. A., Wyithe J. S. B., Schaye J., Duffy A. R., 2015b, MNRAS, 450, 1521
Correa C. A., Schaye J., Clauwens B., Bower R. G., Crain R. A., Schaller M., Theuns T., Thob A. C. R., 2017, MNRAS, 472, L45
Correa C. A., Schaye J., Wyithe J. S. B., Duffy A. R., Theuns T., Crain R. A., Bower R. G., 2018, MNRAS, 473, 538
Crain R. A. et al., 2015, MNRAS, 450, 1937
Creasey P., Theuns T., Bower R. G., 2015, MNRAS, 446, 2125
Croton D. J. et al., 2006, MNRAS, 365, 11
Dalla Vecchia C., Schaye J., 2012, MNRAS, 426, 140
Davé R., Finlator K., Oppenheimer B. D., 2012, MNRAS, 421, 98
Dayal P., Ferrara A., Dunlop J. S., 2013, MNRAS, 430, 2891
Dekel A., Mandelker N., 2014, MNRAS, 444, 2071
De Rossi M. E., Bower R. G., Font A. S., Schaye J., Theuns T., 2017, MNRAS, 472, 3354
Duffy A. R., Schaye J., Kay S. T., Dalla Vecchia C., Battye R. A., Booth C. M., 2010, MNRAS, 405, 2161
Ferrarese L., 2002, ApJ, 578, 90
Furlong M. et al., 2015, MNRAS, 450, 4486
Guo Q., White S., Li C., Boylan-Kolchin M., 2010, MNRAS, 404, 1111
Haas M. R., Schaye J., Booth C. M., Dalla Vecchia C., Springel V., Theuns T., Wiersma R. P. C., 2013a, MNRAS, 435, 2931
Haas M. R., Schaye J., Booth C. M., Dalla Vecchia C., Springel V., Theuns T., Wiersma R. P. C., 2013b, MNRAS, 435, 2955
Hernquist L., 1990, ApJ, 356, 359
Hernquist L., Springel V., 2003, MNRAS, 341, 1253
Hopkins P. F., Kereš D., Oñorbe J., Faucher-Giguère C.-A., Quataert E., Murray N., Bullock J. S., 2014, MNRAS, 445, 581
Kennicutt R. C., Jr., 1998, ApJ, 498, 541
King A., 2003, ApJ, 596, L27
Kormendy J., Ho L. C., 2013, ARA&A, 51, 511
Kravtsov A. V., 2013, ApJ, 764, L31
Krumholz M. R., Dekel A., 2012, ApJ, 753, 16
Lacey C., Cole S., 1993, MNRAS, 262, 627
Lilly S. J., Carollo C. M., Pipino A., Renzini A., Peng Y., 2013, ApJ, 772, 119
Łokas E. L., Mamon G. A., 2001, MNRAS, 321, 155
Loveday J. et al., 2012, MNRAS, 420, 1239
Ludlow A. D., Navarro J. F., Angulo R. E., Boylan-Kolchin M., Springel V., Frenk C., White S. D. M., 2014, MNRAS, 441, 378
Lynden-Bell D., Lynden-Bell R. M., 1977, MNRAS, 181, 405
McAlpine S. et al., 2016, Astron. Comput., 15, 72
McAlpine S., Bower R. G., Rosario D. J., Crain R. A., Schaye J., Theuns T., 2018, MNRAS, 481, 3118
McConnell N. J., Ma C.-P., Gebhardt K., Wright S. A., Murphy J. D., Lauer T. R., Graham J. R., Richstone D. O., 2011, Nature, 480, 215
Magorrian J. et al., 1998, AJ, 115, 2285
Mannucci F., Cresci G., Maiolino R., Marconi A., Gnerucci A., 2010, MNRAS, 408, 2115
Mo H. J., Mao S., White S. D. M., 1998, MNRAS, 295, 319
Mortlock A., McLure R. J., Bowler R. A. A., McLeod D. J., Mármol-Queraltó E., Parsa S., Dunlop J. S., Bruce V. A., 2017, MNRAS, 465, 672
Moster B. P., Naab T., White S. D. M., 2018, MNRAS, 477, 1822
Naab T., Ostriker J. P., 2017, ARA&A, 55, 59
Navarro J. F., Frenk C. S., White S. D. M., 1997, ApJ, 490, 493
Navarro J. F., Benítez-Llambay A., Fattahi A., Frenk C. S., Ludlow A. D., Oman K. A., Schaller M., Theuns T., 2017, MNRAS, 471, 1841
Neto A. F. et al., 2007, MNRAS, 381, 1450
Noeske K. G. et al., 2007, ApJ, 660, L43
Oppenheimer B. D., Davé R., Kereš D., Fardal M., Katz N., Kollmeier J. A., Weinberg D. H., 2010, MNRAS, 406, 2325
Parsa S., Dunlop J. S., McLure R. J., Mortlock A., 2016, MNRAS, 456, 3194
Peacock J. A., Smith R. E., 2000, MNRAS, 318, 1144
Planck Collaboration I, 2014, A&A, 571, A1
Press W. H., Schechter P., 1974, ApJ, 187, 425
Prialnik D., 2009, An Introduction to the Theory of Stellar Structure and Evolution, Cambridge Univ. Press, Cambridge
Reed D. S., Bower R., Frenk C. S., Jenkins A., Theuns T., 2007, MNRAS, 374, 2
Rosas-Guevara Y. M. et al., 2015, MNRAS, 454, 1038
Salcido J., Bower R. G., Theuns T., 2020, MNRAS, 491, 5083
Schaller M. et al., 2015, MNRAS, 451, 1247
Schaye J., Dalla Vecchia C., 2008, MNRAS, 383, 1210
Schaye J. et al., 2010, MNRAS, 402, 1536
Schaye J. et al., 2015, MNRAS, 446, 521
Schechter P., 1976, ApJ, 203, 297
Schreiber C. et al., 2015, A&A, 575, A74
Shibuya T., Ouchi M., Harikane Y., 2015, ApJS, 219, 15

Silk J., Rees M. J., 1998, A&A, 331, L1
Somerville R. S., Davé R., 2015, ARA&A, 53, 51
Song M. et al., 2016, ApJ, 825, 5
Springel V., 2005, MNRAS, 364, 1105
Springel V. et al., 2005, Nature, 435, 629
Strickland D. K., Heckman T. M., 2009, ApJ, 697, 2030
Tacchella S., Bose S., Conroy C., Eisenstein D. J., Johnson B. D., 2018, ApJ, 868, 92
Thornton K., Gaudlitz M., Janka H. T., Steinmetz M., 1998, ApJ, 500, 95
Trayford J. W. et al., 2015, MNRAS, 452, 2879
Trayford J. W., Theuns T., Bower R. G., Crain R. A., Lagos C. D. P., Schaller M., Schaye J., 2016, MNRAS, 460, 3925
Trayford J. W. et al., 2017, MNRAS, 470, 771
Trayford J. W., Frenk C. S., Theuns T., Schaye J., Correa C., 2019, MNRAS, 483, 744
Tremonti C. A. et al., 2004, ApJ, 613, 898
Vale A., Ostriker J. P., 2004, MNRAS, 353, 189
van de Voort F., 2017, in Fox A., Davé R., eds, Astrophysics and Space Science Library, Vol. 430, Gas Accretion on to Galaxies. Springer-Verlag, Berlin, p. 301
van der Wel A. et al., 2014, ApJ, 788, 28
Wechsler R. H., Tinker J. L., 2018, ARA&A, 56, 435
White S. D. M., Frenk C. S., 1991, ApJ, 379, 52
White S. D. M., Rees M. J., 1978, MNRAS, 183, 341
Wiersma R. P. C., Schaye J., Theuns T., Dalla Vecchia C., Tornatore L., 2009, MNRAS, 399, 574

APPENDIX A: SIMULATION DETAILS

We compare the results of the model described in this paper to galaxies from the EAGLE simulation, which we briefly describe here. EAGLE is a suite of cosmological, hydrodynamical simulations, performed using an evolution of the GADGET smoothed particle hydrodynamics code described by Springel (2005). EAGLE uses a set of subgrid modules to encode unresolved physics, described in detail by Schaye et al. (2015), which we briefly summarize here.

The subgrid modules contain a set of numerical parameters, whose values are calibrated in a REFERENCE run to reproduce a small number of $z \approx 0$ observables, namely the GSMF, the relation between galaxy stellar mass, $M_\star$, and size, and between $M_\star$ and black hole mass, as detailed by Crain et al. (2015). Given these calibrated values, the simulation also reproduces several observable relations that were not part of the calibration, in particular yielding a 'main sequence' of blue star-forming galaxies in which $\dot{M}_\star$ depends on $M_\star$ and redshift as observed (Furlong et al. 2015), as well as a 'red sequence' of quenched galaxies (Trayford et al. 2015, 2017). The $z = 0$ galaxy colours correlate with galaxy morphology as observed (Correa et al. 2017; Trayford et al. 2018).

Most relevant for the comparisons in this paper is the implementation of star formation, of stellar feedback, and of feedback from accretion black holes (AGNs) in EAGLE:

(i) *Star formation:* Sufficiently dense gas in EAGLE is converted into star particles at a rate per unit volume, $\dot{\rho}_\star$, that depends on the gas pressure, P, as

$$\dot{\rho}_\star \propto P^{(n-1)/2}. \tag{A1}$$

The normalization of this relation and the exponent n are set by the Kennicutt–Schmidt law (Kennicutt 1998) that relates the surface density of star formation, $\dot{\Sigma}_\star$, and of gas, $\Sigma_{\rm g}$,

$$\dot{\Sigma}_\star = A \left(\frac{\Sigma_{\rm g}}{1\ {\rm M}_\odot\ {\rm pc}^{-2}} \right)^n. \tag{A2}$$

The underlying assumption connecting these relations is that volume and surface densities are related by the local Jeans length, as motivated by Schaye & Dalla Vecchia (2008). The simulation does not resolve the multiphase nature of the ISM and star-forming gas is assumed to have a minimum pressure (Schaye et al. 2015),

$$P \propto \rho^{4/3} \propto u^4, \tag{A3}$$

where u is the thermal energy per unit mass.

(ii) *Stellar feedback* is implemented as described by Dalla Vecchia & Schaye (2012): A newly formed star particle increases the temperature of surrounding gas by an amount ΔT. The quantity of gas heated depends on the effective energy injected by star formation, $f_{\rm th}\Delta E$, where ΔE is the total energy released by the winds from massive stars and core-collapse supernovae, which in turn depends on the assumed stellar initial mass function (IMF). The value of ΔT is chosen such that gas is heated to a temperature where its cooling rate is small: This makes the feedback efficient. The value of $1 - f_{\rm th}$ quantifies the fraction of injected energy that is lost from the star-forming region, for example through radiative cooling; $f_{\rm th}$ is one of the main calibration parameters in EAGLE.

(iii) *Black holes and AGNs:* The seeding, merging, accretion, and feedback from black holes (BHs) in EAGLE is described by Rosas-Guevara et al. (2015). Seed BHs are inserted in each dark matter halo once it becomes sufficiently well resolved. When a BH accretes mass and becomes an AGN, it injects thermal energy in the surrounding gas.

The origin of red galaxies in EAGLE is investigated by Trayford et al. (2016). Ram-pressure stripping and 'strangulation' dramatically decrease the star formation rate of satellite galaxies, causing them to leave the blue cloud of star-forming galaxies and settle on to the red sequence. The simple self-regulating model described in this paper does not attempt to describe these effects, and we will therefore only compare to central, *i.e.* non-satellite, EAGLE galaxies. Similarly, AGN feedback suppresses star formation in massive galaxies, causing them to become passive. Since that mechanism is also not included in the model, most of the comparison in this paper is to EAGLE variation FbConstNoAGN, in which $f_{\rm th}$ is a constant, and which does not include AGN feedback. We also use variation FbConst, in which $f_{\rm th}$ is kept constant and which *does* include an AGN.

Table A1 contains a list of parameters of the EAGLE runs that we used. Simulation 'REF' is the default EAGLE model from table 2 of Schaye et al. (2015). The simulation FBconst with $f_{\rm th} = 1$ appears in table 1 of Crain et al. (2015), simulation. Simulation DMO is a dark matter-only version of the same volume. All simulations are initialized from the same Gaussian initial conditions, so that halo masses are nearly identical in all runs.

Table A1. Selected parameters of the EAGLE simulations used here. From left to right, the columns show: simulation name, comoving box size, initial baryonic particle mass, maximum proper softening length, and comment.

Name	L (Mpc)	$m_{\rm g}$ (10^6 M$_\odot$)	$\epsilon_{\rm prop}$ (kpc)	Comment
REF	50	1.81	0.7	reference model
FBconst	50	1.81	0.7	$f_{\rm th} = 1$
FBconstnoAGN	50	1.81	0.7	$f_{\rm th} = 1$, no AGN
DMO	50	0	0.7	dark matter only

Galaxies of the EAGLE reference model look like observed galaxies in many of their properties. Keeping $f_{\rm th}$ constant, the simulated galaxies have similar stellar masses and star formation rates, but are typically smaller than in the reference model. Therefore, this model is not as good a representation of the real galaxy population, but we believe its physics is still reasonable – and it is much easier to compare to our simple model. Many of the properties of the population of EAGLE galaxies can be extracted directly from the public data base[14] (McAlpine et al. 2016), which we used extensively in preparing the figures.

[14] http://icc.dur.ac.uk/Eagle/database.php.

This paper has been typeset from a TEX/LATEX file prepared by the author.